DETERMINING THE INDICES OF REFRACTION OF REACTIVELY SPUTTERED URANIUM DIOXIDE THIN FILMS FROM 46 TO 584 ANGSTROMS

by

Shannon Lunt

A thesis submitted to the faculty of

Brigham Young University

in partial fulfillment of the requirements for the degree of

Master of Science

Department of Physics and Astronomy

Brigham Young University

August 2002

Copyright © 2002 Shannon Lunt

All Rights Reserved

BRIGHAM YOUNG UNIVERSITY

GRADUATE COMMITTEE APPROVAL

of a thesis submitted by

Shannon Lunt

This thesis has been read by each member of the following graduate committee and by majority vote has been found to be satisfactory.

Date	R. Steven Turley, Chair
Date	David D. Allred
Date	Scott D. Bergeson

BRIGHAM YOUNG UNIVERSITY

As chair of the candidate's graduate committee, I have read the thesis of Shannon Lunt in its final form and have found that (1) its format, citations, and bibliographical style are consistent and acceptable and fulfill university and department style requirements; (2) its illustrative materials including figures, tables, and charts are in place; and (3) the final manuscript is satisfactory to the graduate committee and is ready for submission to the university library.

________________	________________
Date	R. Steven Turley, Chair Graduate Committee

Accepted for the Department

R. Steven Turley, Chair
Department of Physics and Astronomy

Accepted for the College

G. Rex Bryce, Associate Dean
College of Physical and Mathematical Sciences

ABSTRACT

DETERMINING THE INDICES OF REFRACTION OF REACTIVELY SPUTTERED URANIUM DIOXIDE THIN FILMS FROM 46 TO 584 ANGSTROMS

Shannon Lunt

Department of Physics and Astronomy

Master of Science

We have determined the indices of refraction of reactively sputtered thin film UO_2 for the first time below 300 Å. Our measured indices for UO_2 differ from those calculated by atomic scattering factors by about 2. This results in UO_2 thin films with an oxide on top reflecting as well as or better than theoretical calculations for UO_2 thin films. We report the measured indices of refraction for UO_2 and the oxide that formed on top as well as fabrication and characterization techniques used.

ACKNOWLEDGMENTS

I would like to thank Dr. Turley and Dr. Allred for their many hours of help in obtaining and analyzing data. My undergraduates, Danelle Brown, Elke Jackson, Kristi Adams, and Richard Sandberg were of invaluable assistance and this project could not have been completed without their assistance. Raymond Rios, Guillermo Acosta, Ty Robinson were very helpful in various measurements. I would also like to thank all of my friends in the physics department who have helped and encouraged me, especially when my motivation was gone. I would expecially like to thank Takeshi Nakata for his hours of help in preparing this thesis.

Contents

Acknowledgments **vi**

List of Tables **ix**

List of Figures **xi**

1 Introduction **1**

1.1 Interest in the Extreme Ultraviolet Region 1

1.2 Project Background 2

1.3 Theory of Reflection in the EUV 3

1.3.1 Optical Constants - Equations 4

1.3.2 Experimental Determination of Constants 6

1.3.3 Project Focus 6

2 Film Deposition **9**

2.1 Sputtering 9

2.2 Deposition Rates 13

2.3 Uniformity 13

3 Characterization **17**

3.1 X-ray Diffraction (XRD) 18

3.2 Ellipsometry 21

3.2.1 Theory 21

3.2.2 Models 22

3.3 X-ray Photoelectron Spectroscopy (XPS) 23

3.3.1 Basic Theory 24
3.3.2 Comparison with Published Data 24
3.3.3 Oxidation Study 27
3.3.4 Sampling Depth 30
3.3.5 Composition of Samples 31
3.4 Atomic Force Microscopy (AFM) 34

4 Reflectance 37

4.1 BYU Data Acquisition 37
4.2 BYU Data 39
4.3 ALS Data Acquisition 40
4.4 ALS Data 43
4.5 Data Analysis 50

5 Conclusion 57

Appendix A 59

List of Tables

2.1 Film Uniformity Study 14

3.1 Density of U, UO_2, and γ-UO_3 18

3.2 Thicknesses of Samples Studied 19

4.1 Optical Constants for UO_2 from BYU Data 40

4.2 Optical Constants for Top Oxide from BYU Data 40

4.3 Optical Constants for UO_2 49

4.4 Optical Constants for Top Oxide Layer 49

4.5 Study of n and k from Ellipsometry 51

4.6 Thickness Fit from Ellipsometry 53

4.7 Fit of XRD Data for Sample UO12 55

List of Figures

1.1 Range of Optical Constants for UO_2 from Literature 3
1.2 Reflection from Multiple Surfaces 4
1.3 Films to be Studied 7
2.1 Cartoon of Sputtering System 10
2.2 Sputter System and Controls 11
2.3 Sputtering Geometry Used 13
3.1 Thickness of Sample UO12 from XRD 20
3.2 XPS Scan of the Oxygen 1s Peak in Uranium Oxides 26
3.3 XPS Scan of the Uranium 4f Peaks in Uranium Oxides 26
3.4 XPS Scan of Sample 1 O1s Peak - 2 Weeks after Deposition 27
3.5 XPS Scan of Sample 2 O1s Peak - 2 Weeks after Deposition 27
3.6 XPS Scan of Sample 1 O1s Peak after 18 Weeks 28
3.7 XPS Scan of Sample 2 O1s Peak after 13 Weeks 28
3.8 XPS Scan of Sample 1 O1s Peak after 26 Weeks 28
3.9 XPS Scan of Sample 1 U4f Peaks after 2 Weeks 28
3.10 XPS Scan of Sample 2 U4f Peaks after 2 Weeks 28
3.11 XPS Scan of Sample 2 U4f Peaks after 13 Weeks 29
3.12 XPS Scan of Sample 1 U4f Peaks after 18 Weeks 29
3.13 XPS Scan of Sample 2 U4f Peaks after 25 Weeks 29
3.14 XPS Scan at 55° of Sample 2 U4f Peaks after 25 Weeks 30
3.15 XPS Scan at 75° of Sample 2 U4f Peaks after 25 Weeks 30
3.16 Depth Profile with Angle for XPS 31
3.17 XPS for Sample UO11 33

3.18 XPS for Sample UO12 33
3.19 XPS for Sample UO13 33
3.20 XPS for Sample UO14 33
3.21 XPS for Sample UO15 33
3.22 Thickness of Uranium Samples from AFM 35
3.23 Roughness of Uranium Samples from AFM 36
4.1 McPherson Monochromator and O-chamber 38
4.2 Reflectance Curve with Good Alignment on the Monochromator . . 38
4.3 Reflectance Curve with Poor Alignment on the Monochromator . . 38
4.4 Reflectometer at the ALS 41
4.5 View of the Synchrotron Ring at the ALS 42
4.6 Effect of Different Filters on Reflection Data from ALS 42
4.7 Geometry for Reflection from a Multilayer 44
4.8 UO_2 δ 47
4.9 UO_2 β 47
4.10 Top Oxide Layer δ 48
4.11 Top Oxide Layer β 48
4.12 Comparison of Reflection Measurements at the ALS at 300 Å and at BYU at 304 Å 50
4.13 Fit for UO13 of Ψ and Δ with an Oxide on top, MSE=2.7449 . . . 52
4.14 Values for n from Ellipsometry 54
4.15 Values for k from Ellipsometry 54
4.16 XRD Fit for Sample UO12 56
4.17 XRD Fit for Sample UO13 56

Chapter 1

Introduction

1.1 Interest in the Extreme Ultraviolet Region

The extreme ultraviolet (EUV), a lesser explored region of the electromagnetic spectrum from about 100–1000 Å, has become very important in the last decade. In the computer industry, there is interest in making smaller and faster chips. The limit has almost been reached of the size of features that can be fabricated using current photolithography technology. Using 110–130 Å light, though, features of 180 Å can be produced, greatly increasing the speed of chips. This technology is called EUV lithography. With this technique, the size of lines that can be resolved will decrease from 500 Å to 160 Å in a few years, increasing the chip speed to 10 GHz. To fabricate the chips, a step and scan method is utilized in which a mask is illuminated by EUV light. Using focusing optics, the image is then shrunk fourfold and the features are reproduced on the substrate. Attwood [1, 2] reports that soon it will be possible to make 80 12-inch wafers in an hour by this process with up to 90 chips on each wafer.

Biological and medical research have also found a use for shorter wavelengths from this range. There is always a search for methods of imaging smaller features in the body to determine biological processes. Previous methods have involved complex sample preparation and the dehydration and staining of samples. Soft x-ray microscopy uses light in the water window, the region from 23.4–43.8 Å where carbon is opaque and water is reasonably transparent, to image cells. The

water window will be considered part of the EUV for the purposes of this work. Using light in this band, it is possible to directly image thick hydrated biological material in a near-native environment [1]. This technique allows imaging of structures from approximately 25 nm up to 10 μm in diameter [1, 3].

Interest has also increased for astronomical observations in the EUV and soft x-ray regions. One example of research in this field is the IMAGE (Imager for Magnetopause-to-Aurora Global Exploration) project, part of a mission to explore the magnetosphere of the earth [4]. By viewing the 304 Å light resonantly scattered from singly ionized He in the earth's magnetosphere, information about interruptions to satellites can be obtained and possible disturbances can be avoided. X-ray astronomers are also interested in the EUV/soft x-ray regions for various purposes, such as viewing the background of the universe [5].

1.2 Project Background

While building mirrors at BYU for the IMAGE satellite, our research group showed that uranium multilayer mirrors with a uranium oxide cap, found to be mostly UO_2, reflected more than expected at 304 Å and greater than many other materials in this region [6]. This opened up the possibilities for using uranium and/or uranium oxides to produce high reflectance multilayer mirrors for the EUV.

From the IMAGE project, we learned that uranium readily oxidizes in air, with an oxidation rate of $12.52 \ln t - 31$ Å/sec, where t is the time in seconds, or about 40 Å in 5 minutes at room temperature [7]. Thus, past measurements of the index of refraction of uranium included a thin oxide layer, leading to inconsistencies and inaccuracies in the data. Our mirrors for the IMAGE project were made with uranium stabilized by a UO_2 cap [6]. The cap not only made the uranium-containing layer more stable by not allowing it to oxidize, it also prevented the oxygen from readily diffusing to the layers below. Also, the cap allowed the mirrors to have a material with a high Z at the top of the stack, allowing for peak

reflectance. These findings increased our interest in using the oxides of uranium in the fabrication of mirrors to be used in space.

1.3 Theory of Reflection in the EUV

Central to the design of mirrors in the EUV is the index of refraction. The contrast in the index of refraction between the materials used in a multilayer mirror helps determine the thicknesses of the various layers. Knowing the index of refraction well means that theory and experiment should agree rather closely. Unfortunately, this is not the case in the EUV as this region of the spectrum has not been thoroughly studied. Weaver, Henke, and Chantler have compiled tables of the optical properties of most of the elements and some compounds using various models [8, 9, 10]. Values from these and other sources do not agree and there are gaps in the EUV data where the indices of refraction of some materials have never been reported. For example, no data exists on the optical properties of uranium dioxide between 10 Å and 310 Å, as shown in Figure 1.1.

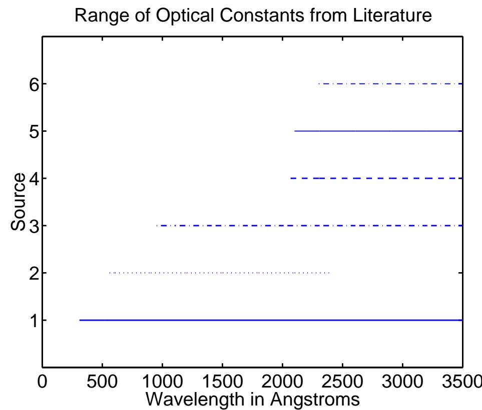

Figure 1.1: 1. Naegele, et. al. [11], 2. Griffiths and Hubbard [12], 3. Schoenes [13], 4. Hubbard and Griffiths [14], 5. Ackermann, et. al. [15], 6. Companion and Winslow [16]

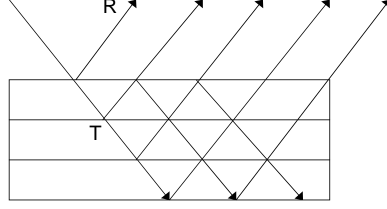

Figure 1.2: Reflection from Multiple Surfaces

The complex index of refraction of a material is

$$N = n + ik \ , \tag{1.1}$$

where n is the real part of the index of refraction and k is the imaginary part or the absorption coefficient. For all materials in the EUV, the real part of the index of refraction is very close to 1, the index of vacuum. As a result, n is written as $1-\delta$, with δ very small. The value of δ at 304 Å for molybdenum, a common material used in multilayers, is 9.5862×10^{-02} [17]. The absorption, k, in this region is fairly large and is often written as β. The value of β for molybdenum at 304 Å is 4.2986×10^{-01} [17]. This means that it is very difficult to get high reflectance from a surface in the EUV due to its low index of refraction and high absorption. In order to get higher reflectance, multilayer films are used with the result that the reflection from each surface adds, as shown in Figure 1.2.

Determining the order of layers and the relative thicknesses of each are some of the difficulties of making mirrors in this region. These techniques have been extensively studied and methods have been developed for theoretically designing the optimum mirror for a certain wavelength [18, 19].

1.3.1 Optical Constants - Equations

Following are equations from Spiller [18] that are useful in determining optical constants in the EUV. The imaginary index of refraction was defined in

Equation 1.1. The index of refraction is also related to the dielectric constant, $\epsilon = \epsilon_1 + i\epsilon_2$, as follows:

$$\epsilon_1 = (1-\delta)^2 - \beta^2 \tag{1.2}$$

$$\epsilon_2 = 2(1-\delta)\beta \ . \tag{1.3}$$

One can use δ and β as calculated from ϵ_1 and ϵ_2 to define the atomic scattering factor, $f = f_1 - if_2$, which is related to the number of free electrons in the material. Values for f_2 can also be calculated from absorption data, as shown in Equation 1.5, and f_1 is found from f_2 using Kramers-Kronig relations [20]. This calculation assumes that f_2 is known for a large number of wavelengths in order to calculate f_1. The atomic scattering factor is related to the index of refraction as follows [1]:

$$\delta = \frac{n_a r_e \lambda^2}{2\pi} f_1 \tag{1.4}$$

$$\beta = \frac{n_a r_e \lambda^2}{2\pi} f_2 \ , \tag{1.5}$$

where n_a is the atomic density, λ is the wavelength of light, and r_e is the classical electron radius defined as

$$r_e = \frac{e^2}{4\pi\epsilon_0 mc^2} \ , \tag{1.6}$$

which is equal to 2.82×10^{-13} cm. These equations are defined for atoms using the Drude theory. To calculate the atomic scattering factors for a compound, the density for the compound is used in place of the atomic density. Using this method for compounds, one can use the atomic scattering factors to calculate δ and β, but this method does not work in reverse.

The Kramers-Kronig relations connect the real and imaginary parts of the atomic scattering factor. These relations are based on the causality relations between the polarization and the electric field in a uniform isotropic medium. Arfken [21] gives the following form for the Kramers-Kronig relations:

$$f_1(\omega_0) = \frac{2}{\pi} P \int_0^\infty \frac{\omega f_2(\omega)}{\omega^2 - \omega_0^2}\, d\omega \tag{1.7}$$

$$f_2(\omega_0) = \frac{2}{\pi} P \int_0^\infty \frac{\omega_0 f_1(\omega)}{\omega^2 - \omega_0^2} \, d\omega \ . \tag{1.8}$$

When ω is equal to ω_0, it is called a resonance and the integral does not exist as the denominator goes to zero. This makes it very difficult to calculate the indices of refraction near a resonance. Kramers-Kronig analysis of indices of refraction is beyond the scope of this thesis.

1.3.2 Experimental Determination of Constants

One method of determining the absorption constant, β, is to measure the intensity of light transmitted through a sample. By comparing the initial intensity, I_0, with the transmitted intensity, I, and knowing the thickness, z, one can calculate the linear absorption coefficient, α, as follows:

$$I = I_0 e^{-\alpha z} \ . \tag{1.9}$$

The linear absorption coefficient is related to the absorption constant, β, as follows:

$$\alpha = \frac{4\pi\beta}{\lambda} \ . \tag{1.10}$$

For molybdenum at a wavelength of 304 Å, $\beta = 4.2986 \times 10^{-1}$ and α is then calculated to be 1.78×10^{-2} Å^{-1}.

From measurements of β at multiple wavelengths, δ can be calculated using the Kramers-Kronig relations. The real part of the index of refraction, $n = 1 - \delta$, as well as β, can also be directly calculated from reflectance measurements, the method used in this work. Other methods for experimentally determining optical constants are listed in Spiller [18].

1.3.3 Project Focus

The focus of this work was experimentally determining the indices of refraction for thin-film UO_2 in the EUV from 45 to 600 Å. The films studied were deposited on Si wafers as shown in Figure 1.3. Chapter 2 will discuss the fabrication of the uranium oxide thin films used in this study. Characterization of the

UO_x

UO_2 – thin film

SiO_2

Si - substrate

Figure 1.3: Films to be Studied

samples will be discussed in Chapter 3. Chapter 4 will discuss reflectance data and the optical constants obtained for UO_2 in the EUV.

Chapter 2

Film Deposition

The surface of oxides formed on metals in air may be rough, causing scattering when measuring the reflectance of a sample. This could greatly decrease the accuracy of our measurements and make it more difficult to determine the optical constants of the material. As a result, I developed a method of producing uranium dioxide thin films that are smoother than a film allowed to oxidize in air. This was possible using a method referred to as reactive sputtering, in this case sputtering uranium in the presence of oxygen [22]. Roughness of samples will be further discussed in Chapter 3.

2.1 Sputtering

Sputtering must take place in a system under moderate vacuum, approximately $1 - 3 \times 10^{-3}$ torr. We evacuated the chamber down to about 4×10^{-6} torr and then shuttered the system before sputtering. The shutter is a metal plate inside the sputter system that swings over the hole leading to the cryopump, decreasing the throughput of the pump so it would not overload when adding gases to the chamber and also increasing the pressure in the chamber. Targets made of the materials to be sputtered are placed on top of a gun. In our system, two guns are located at the bottom of the chamber and a sample tray is at the top of the chamber. Argon is introduced to the chamber and a negative voltage is applied to the guns with the sample tray grounded. The voltage applied to the guns ionizes the Ar and the ions hit the negatively charged targets, knocking off atoms which

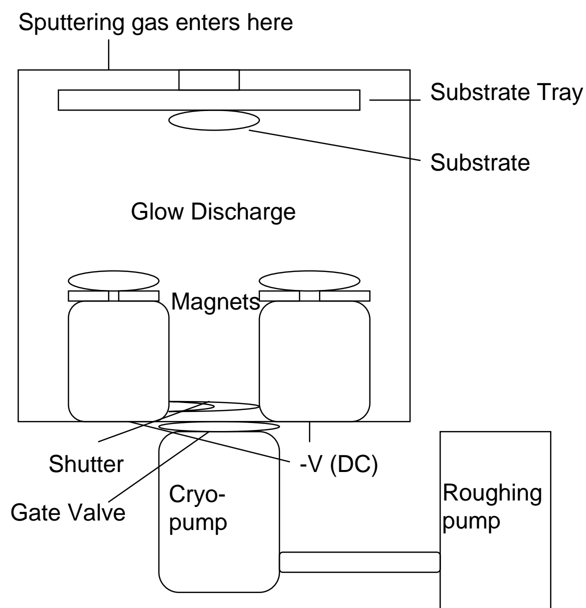

Figure 2.1: DC Magnetron Sputtering

deposit on the sample above. Magnets are placed beneath the targets to contain the electrons within the Ar plasma to the region directly above the targets. This allows the samples to be sputtered at a lower system pressure and increases the deposition rate. The sample tray is slowly rotated over the targets to deposit films of desired thicknesses. This technique is called DC magnetron sputtering. Our samples were made by combining this technique with reactive sputtering. A cartoon of the sputter system is shown in Figure 2.1. Figure 2.2 shows the sputter system and high voltage control.

Our method of reactive sputtering entailed adding oxygen and argon to the chamber and controlling the partial pressures by mass flow controllers. As argon and oxygen are added to the chamber, the oxygen combines with uranium on all exposed surfaces, including the surface of the target. The argon atoms then knock off both uranium and oxygen atoms which deposit a smooth film of uranium dioxide on the substrate. By controlling the partial pressures of Ar and O_2 entering into the system, the composition of the oxide formed may be controlled. That is,

Figure 2.2: Sputter System and Controls

we operated in a mode where there was just more than enough oxygen to oxidize the uranium as it was exposed. The argon pressure we used during sputtering was about 4×10^{-3} torr and the oxygen pressure was 3×10^{-4} torr. The partial pressures of Ar and O_2 were set by a Barocel® capacitance manometer and mass flow controllers and read by a multipole analyzer (MPA).

From previous experience, we know the values of the voltage, approximately 440 V, and the current, approximately 189 mA, for sputtering a pure uranium target. When first attempting reactive sputtering of uranium in O_2, the voltages and currents were much different than the values expected for sputtering pure uranium, approximately 700 V and 114 mA. This appears to be due to excess oxygen in the chamber resulting in the target surface being oxidized to a large depth. The large oxide layer causes the resistance of the target to be higher than for pure uranium and the sputter rate to be lower. After a few minutes of sputtering in oxygen-free argon, the oxide surface layers on the target are removed and the current rises as the resistance of the target falls. The power supply lowers the supplied voltage to maintain a constant power of 83 W.

The voltage was about 442 V and the current was 189 mA for the samples used in this work. Interestingly, these are approximately the same values as those obtained for pure uranium sputtered in an oxygen-free atmosphere but the sputter rate is much less. When reactively sputtering a material in O_2, two situations could occur. First, the oxygen combines with the target resulting in the surface layer being a compound. The compound is sputtered and deposits together onto the substrate. Second, the target atoms and oxygen deposit independently on the sample resulting in areas of different stoichiometry. X-ray photoelectron spectroscopy measurements of the deposited films showed that the stoichiometry was close to UO_2 and it was assumed that the target was oxidized to UO_2 with the compound being sputtered. Since UO_2 was the desired stoichiometry, subsequent films made used the O_2 pressure, about 3×10^{-4} torr, required to have the voltage and current values of about 440 V and about 189 mA.

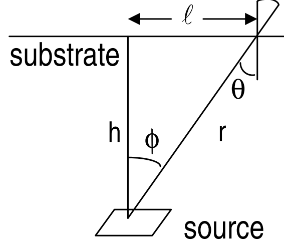

Figure 2.3: Sputtering Geometry after [22]

2.2 Deposition Rates

To be able to replicate samples by sputtering, the deposition rates must be known and the conditions of deposition must be the same. The amount of Ar and O_2 added to the chamber was kept the same for each sample by comparing the voltages read by the Barocel® and the partial pressures measured by the MPA. The voltage and current were also kept constant for the various samples by controlling the O_2 pressure. The time that the sample was kept over the gun determined its thickness. For example, a sample that was scanned over the uranium target for 1000 seconds produced a film of UO_2 that was approximately 140 Å thick, as measured by X-ray diffraction. This would give a sputter rate of 0.14 Å/sec.

2.3 Uniformity

In sputtering, the relative position of the source and substrate is important for film thickness uniformity. To achieve films of uniform thickness, the source and substrate should be located on a sphere so that all parts of the substrate are equidistant from the source during sputtering. If this is not the case, as it is not in our system as shown in Figure 2.1, the edges of the sample will be different thicknesses than the middle. If the source is a surface, rather than a point, and the geometry is as in Figure 2.3, the total mass, M_e deposited from a source of area A_e can be calculated as follow from Ohring [22]:

$$M_e = \int_0^t \int_{A_e} \Gamma_e \, dA_e \, dt \ , \tag{2.1}$$

Γ_e is the mass evaporation rate defined as $\Gamma_e = 5.834 \times 10^{-2}\sqrt{M/T}P_e$ g/cm^2-sec. For a surface source, the mass deposited per unit area is given by

$$\frac{dM_s}{dA_s} = \frac{M_e \cos(\phi)\cos(\theta)}{\pi r^2} \ . \tag{2.2}$$

The thickness, d, of the film at any distance, l, from the center of the wafer can be calculated as

$$d = \frac{M_e \cos\theta \cos\phi}{\pi \rho r^2} = \frac{M_e}{\pi \rho r^2}\frac{h}{r}\frac{h}{r} = \frac{M_e h^2}{\pi \rho (h^2 + l^2)^2} \ , \tag{2.3}$$

where ρ is the density of the deposit. The greatest thickness on the sample will be when $l = 0$ or

$$d_0 = \frac{M_e}{\pi \rho h^2} \ . \tag{2.4}$$

Normalizing the sample thickness then gives

$$\frac{d}{d_0} = \frac{1}{(1 + (l/h)^2)^2} \ . \tag{2.5}$$

Table 2.1 gives some values for d and d_0 for thin films that are similar to those we studied. In this case, $l = 2$ inches, as we used 4-inch diameter wafers, and $h \approx 25$ cm or 9.84 inches, giving a value $d/d_0 = 0.922$. As can be seen from Table 2.1, the differences in thickness across the wafer can vary by up to 20 Å. This can lead to discrepancies in characterizing the thickness of the film by different methods if different parts of the sample are used.

Table 2.1: Film Thickness at the Center, d_0, and Edge of the Wafer, d

d_0 (Å)	d (Å)
50	46.1
100	92.2
150	138.3
200	184.4
250	230.5

When uniformity of the film is a concern, this variation in the thickness across the sample must be compensated for. One method is to mount the substrate on a holder with a motor that spins the sample as the material is being sputtered. Also, masks must be used on the target to direct the sputtering materials toward a small part of the substrate at a time. The exact shape and size of the mask must be determined by experiment and partially depends on the sputter rates of the materials. It was decided for this study that uniformity of the films was not an essential characteristic for determining optical constants so no compensations were made for this effect. As a result of the variations in thickness across the sample, though, characterization measurements were made in the center of the sample, if possible.

Chapter 3

Characterization

In order to calculate optical constants for our samples, we had to have a good model which included the composition, thickness of the layers, and roughness. Several characterization techniques were used to determine this information. X-ray diffraction was used at near-grazing angles to calculate an approximate thickness for the samples. This technique is especially useful for thinner samples, approximately thinner than 150 Å. Ellipsometry was used to gain another approximation on the thickness as well as the optical constants of the film in the ultraviolet. Unfortunately, this method is strongly dependent on the model used for the film. Also, the ellipsometer used takes data in atmosphere, so the sample continues to oxidize during measurements, but it only takes a few minutes to take a complete set of data for a sample. X-ray photoelectron spectroscopy was used to determine the composition of the films by comparing the position of certain peaks with data from the literature. Atomic force microscopy was the most direct measurement we had available. This technique allowed us to measure the roughness of a sample over a small range, such as a μm, and also was used to measure thicknesses. This thickness measurement should help determine the thickness of our films more exactly when used in conjunction with x-ray diffraction. The only drawback to this technique is that it is conducted in atmosphere so the sample continues to oxidize as the data is being taken. As the films oxidize they swell due to a change in density. The densities of uranium and two of its oxides are shown in Table 3.1

Table 3.1: Density of U, UO_2, and γ-UO_3

Material	Density (g/cm^3)
U	18.95
UO_2	10.96
γ-UO_3	7.3

3.1 X-ray Diffraction (XRD)

XRD can be used to determine thicknesses of samples. Copper K-α radiation of 1.5406 Å is scattered off a sample and the resulting intensity is detected at near-grazing angles. The data tells us how the light is diffracted from the surface, which to first order can be represented by Bragg diffraction from a single surface, $m\lambda = 2d \sin\theta$, where m is the diffraction order, λ is the wavelength of incident radiation in the material or λ_0/n, d is the thickness of the film, and θ is the angle between the incident and refracted beam. From the difference in position in angle of the various orders of the diffraction peaks, a rough estimate of the thickness, d, of the film can be calculated. By taking the difference between the peaks, any phase shifts that occur at interfaces are taken into account. If the films being studied are thin, on the order of a few hundred Å's, XRD is only measured for low angles. In our case, measurements were taken using a Scintag X-ray diffractometer between 0.6° and 5°, 2θ.

Using a program by David Windt called IMD [23] we were able to find the approximate thicknesses of the films. A model of the thin film was built in IMD using optical constants from a database included in the program for Si and SiO_2 and constants from the CXRO website [17] for UO_2. The CXRO website uses atomic scattering factors calculated from absorption measurements used in Henke [9]. Then the XRD data was read into IMD and compared with the reflection of the model. The thickness of the UO_2 layer in the model was changed until the peaks and minima of the reflectance vs. angle plot matched. An example of this

Table 3.2: Thicknesses of Samples Studied

Sample	Thickness Desired (Å)	Thickness from XRD (Å)
UO11	50	60
UO12	110	111
UO13	185	185
UO14	225	-
UO15	250	-
UO16	35	-

match is shown in Figure 3.1. Further studies on XRD and better fits can be found in Section 4.5.

XRD was done on samples UO11, UO12, and UO13. Due to construction on the Eyring Science Center, we were unable to do XRD on the last three samples before reflection measurements were taken. Since the first three samples appeared to be very close to the thickness desired, the sputter rate was assumed to be constant for all samples and the thicknesses were assumed to be the same as the desired thicknesses. The thicknesses determined by XRD and desired for each sample are shown in Table 3.2.

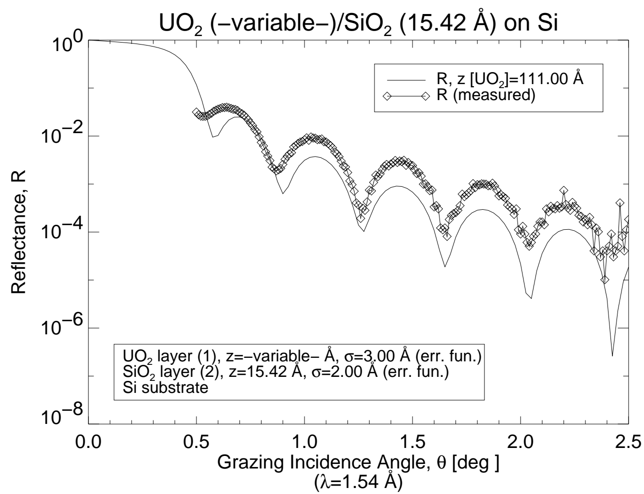

Figure 3.1: Finding the Thickness of Sample UO12 in IMD from XRD Data

3.2 Ellipsometry

3.2.1 Theory

Ellipsometry uses polarized light to determine sample thicknesses or indices of refraction. This is done by measuring the polarization of light reflected off of a sample. With a rotating analyzer ellipsometer, the source is linearly polarized, reflected off a sample, passed through the continuously rotating analyzer, and then the resulting polarization is detected. From the signal at the detector, which is the light converted to DC voltage, one is able to determine the polarization of the beam reflected from the sample. If the beam at the detector is constant, the light reflected from the sample was circularly polarized. If the light reflected off the sample is sinusoidal, the polarization after the sample was elliptical [24].

Reported values from ellipsometry are Ψ and Δ. The ellipsometer is able to measure the ratio in amplitude of the s- and p-polarized light reflected from the sample as Ψ. The difference between the imaginary parts of the different polarizations or the phase difference is Δ. The quantities Ψ and Δ are related to the ratio of the Fresnel reflection coefficients R_s and R_p as follows:

$$\frac{R_p}{R_s} = \tan(\Psi)e^{i\Delta} \ . \tag{3.1}$$

From the Ψ and Δ calculated by the ellipsometer, one can obtain the indices of refraction, n and k, or the thickness. This technique is superior to others in that it can measure the phase, Δ, and not just the intensity of the reflected beam.

We used an M2000D spectroscopic ellipsometer with a rotating compensator (or rotating analyzer) from the J. A. Woollam Company for the UV, allowing a range of wavelengths from 189 nm to 1000 nm (1.24 eV to 6.55 eV) [25]. Measurements can be taken at various angles, as well. This allows for more data to be taken and makes it possible to fit the optical constants at each wavelength in the desired range.

Even though we cannot obtain indices of refraction in the desired range of 25–600 Å using our ellipsometer, this data is useful in checking the constants

we obtain against published data. Also, ellipsometry can be used to check the thickness of our samples as obtained by XRD.

3.2.2 Models

To calculate optical constants from ellipsometric data, the model used is essential. A usual model for situations where electrons are nearly free, such as in metals and in materials at high energies, is the Lorentz oscillator model. This model represents the interaction of light with an electron in an atom as a damped harmonic oscillator. The Lorentz model gives the following equation for the dielectric constant of a material [20]:

$$\frac{\epsilon(\omega)}{\epsilon_0} = 1 + \sum_j \frac{Ne^2 f_j}{\epsilon_0 m(\omega_j^2 - \omega^2 - i\omega\gamma_j)} \ . \tag{3.2}$$

This equation supposes that there are N molecules per unit volume, Z electrons per molecule, and f_j electrons per molecule with binding frequency ω_j and damping constant γ_j. The Lorentz model is particularly useful for resonant absorptive processes.

In cases where the band gap is outside of the measurement range, a Cauchy model with k can be used. The Cauchy dispersion relation is good for parametrization of the index of transparent materials, or regions where $k = 0$. One form of this relation is

$$n(\lambda) = A + B/\lambda^2 + C/\lambda^4 + \dots \ , \tag{3.3}$$

where λ is measured in μm and A, B, and C are the fitting parameters. This model is good for films thicker than about 100 Å. In heavy metal oxides, such as uranium oxides, band gaps are generally smaller than those of light oxides, typically less than 6 eV. In addition, in UO_2, two 5f electrons above the 6p closed shell are left with the atom, producing absorption in the uranium oxide gap. This absorption starts at about 2 eV [26] and is well within the measurement range of our ellipsometer.

The model we used is called a general oscillator model because it allows the use of several different types of oscillators at a time. This is because experiment showed that ϵ for an oxide cannot be fit exactly by single oscillator models. Some of the functions available in the general oscillator model are as follows: Lorentz, Tauc-Lorentz, Gauss-Lorentz, Cauchy, harmonic, and Gaussian. The general oscillator model is also more powerful in that it allows the use of a band gap in the model. A band gap is a wavelength range where the material is nonabsorbing or $k = 0$. Oxides are typically wide band gap materials so the general oscillator model is especially useful when modelling the optical constants of oxides. The general oscillator method is described in an update to the ellipsometer manual [24]. From our calculations, this model seems to give the most reasonable optical constants in the UV for UO_2 on SiO_2 on Si. In this region, the value for k goes to zero within the band gap of UO_2 and is small over the whole region.

3.3 X-ray Photoelectron Spectroscopy (XPS)

XPS is one of several techniques available for determining surface composition of samples. Other techniques include Auger electron spectroscopy (AES), secondary ion mass spectrometry (SIMS), Rutherford backscattering (RBS), and scanning electron microscope-energy dispersive x-ray (SEM/ EDX). A comparison of these techniques can be found on page 275 of [22]. XPS was the only technique available at BYU at the time the data was collected for this work. The BYU Department of Chemistry has since acquired a secondary ion mass spectrometer (SIMS) that can help with the compositions of films and will be able to provide information about the amount of hydrogen in the sample, useful in determining the stoichiometry of samples. Of these techniques, though, only XPS is capable of readily giving information on the nature of chemical bonds and the valence states of the sample constituents. We used XPS to find exactly that information, so for us it was the optimal technique for chemical characterization.

3.3.1 Basic Theory

In XPS the sample is bombarded by either aluminum (1487.7 eV) or magnesium (1253.6 eV) K-α x-rays and the kinetic energy of ejected electrons is measured. The difference between the initial energy of the photons and the kinetic energy of the ejected electrons is the binding energy, characteristic of the elements in the sample. From these measurements, information can be obtained about the relative abundance of different elements in a sample and its approximate chemical composition.

In taking XPS data, one must calibrate the system or use a known peak to compensate for any drift in the measured energies for measurements taken at different times. The carbon 1s peak at a binding energy of 285 eV is often used because adventitious carbon is always present on the surface of samples that have been exposed to the atmosphere [27, 28, 29]. Our system was calibrated using a gold or copper sample once a month. Another difficulty arises with insulating samples as the surface charges during the XPS measurement, resulting in all of the binding energies shifting to higher values by as much as 3–10 eV [27]. Veal and Lam [30], though, state that UO_2 should be a conductor at room temperature so there should be no charge buildup during XPS. We agreed with Veal and Lam that UO_2 should not have a charge buildup so use of an electron flood gun to neutralize the sample was not needed.

3.3.2 Comparison with Published Data

Many studies have been done of the XPS spectra for various uranium oxides. These studies show how the type of oxide present can be determined by the difference in position of the various uranium peaks [27, 28, 29, 31, 32, 33, 34, 35]. Other studies have focused on detailed features of the spectra of specific uranium oxides [30, 36, 37].

Allen and Holmes [27] determined from XPS data that the oxide that forms on UO_2 at 25°C is amorphous UO_3. The XPS data obtained for our samples was studied to see how much UO_2 and UO_3 were present. Studies were also done as the samples aged to see how the composition changed with time. The articles by Teterin, et. al. [35] and Allen and Holmes [27] were used extensively in this study as they appear to be the most complete analyses of uranium oxidation states by XPS.

In analyzing the XPS data obtained for our films, we used the data cited in [27, 35] to determine the oxidation state of our films from the position of the peaks. The position of the uranium $4f_{5/2}$ and $4f_{7/2}$ peaks along with the position of the oxygen 1s peak are most helpful in determining composition as they change with the different amounts of oxide and the peaks are very intense. The change in the oxygen 1s peak with an increase in oxidation state can be seen in Figure 3.2. From Figure 3.3, one can see that the peaks shift to higher binding energies with increased oxidation. Also, other structures appear as a result of more or less oxygen and different valence states of uranium. For example, in the 4f peaks, the distance from the fundamental line to satellites is characteristic of the chemical bond and is not the same for different oxides. Therefore, the change in this distance can be used to determine the exact oxide.

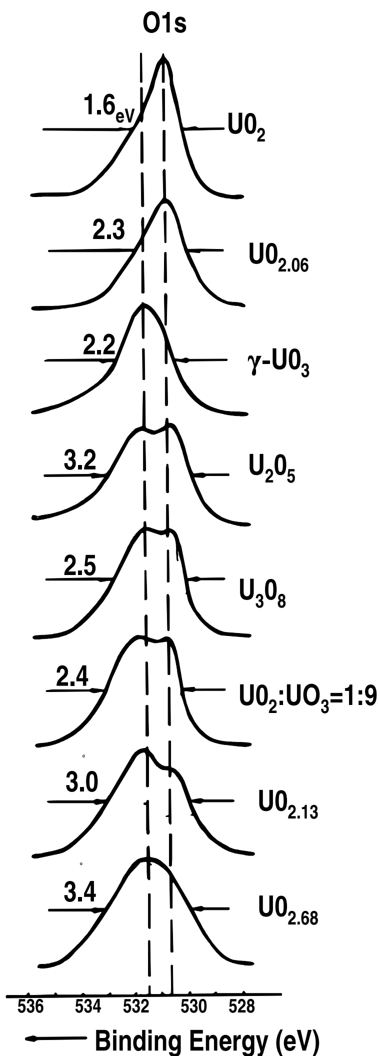

Figure 3.2: XPS Scan of O1s Comparing Binding Energies in eV [35]

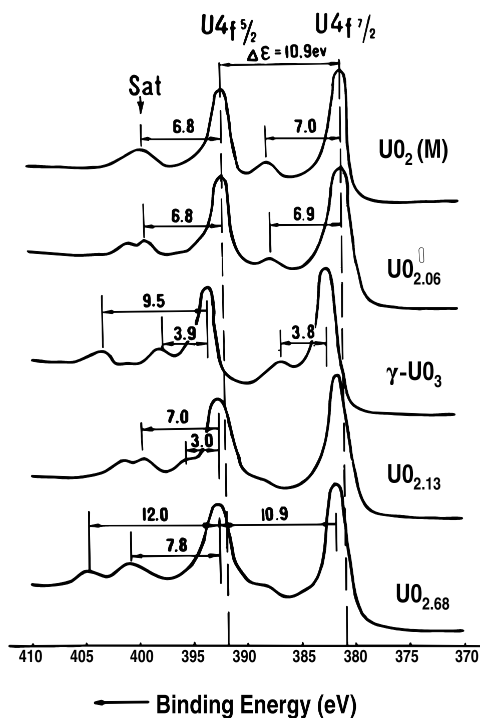

Figure 3.3: XPS Scan of U4f Comparing Binding Energies in eV [35]

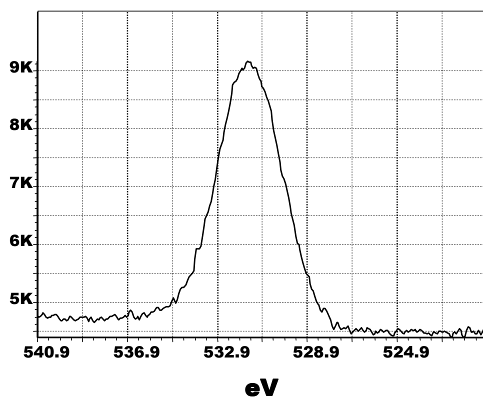

Figure 3.4: XPS Scan of Sample 1 O1s Peak - 2 Weeks after Deposition

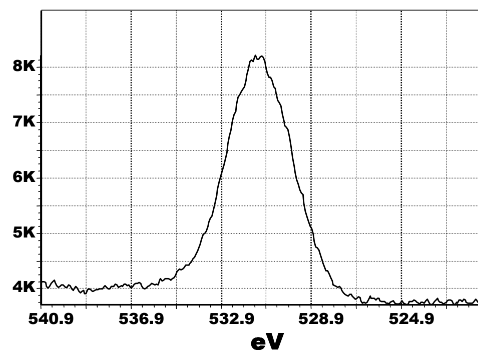

Figure 3.5: XPS Scan of Sample 2 O1s Peak - 2 Weeks after Deposition

3.3.3 Oxidation Study

We have examined two thin films of uranium oxide to determine their composition and how it changes as the films are exposed to atmosphere at room temperature. Figures 3.4 and 3.5 show the oxygen 1s peak of the samples two weeks after they were produced.

Two weeks after creation, the thin films showed a mixture of half UO_2 and half UO_3. Figures 3.6, 3.7, and 3.8 show the oxygen 1s peak after the films had been exposed to atmosphere at room temperature for a few months. These graphs show that as the films were allowed to oxidize, the higher energy peak became more intense while the lower energy peak diminished.

The uranium $4f_{5/2}$ and $4f_{7/2}$ peaks were also studied to verify oxidation states. Figures 3.9 and 3.10 show these peaks for the samples two weeks after creation.

One can see from Figures 3.11, 3.12, and 3.13 that as the films were exposed to atmosphere at room temperature, the uranium peaks shifted to lower energies for at least the first 18 weeks, but then the trend began to shift to higher energies.

Figure 3.4 through Figure 3.13 were produced by XPS scans with an incident angle of 55 degrees. To observe whether a different spectra was produced with

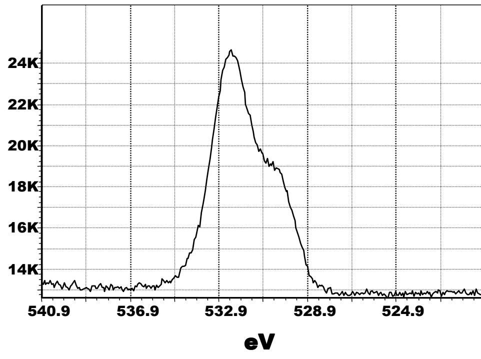

Figure 3.6: Sample 1 after 18 Weeks

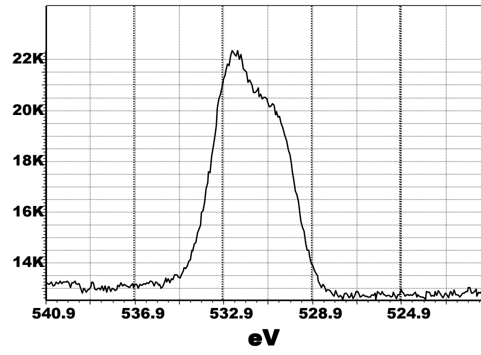

Figure 3.7: Sample 2 after 13 Weeks

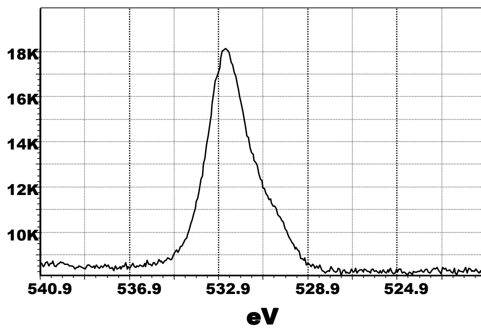

Figure 3.8: Sample 1 after 26 Weeks

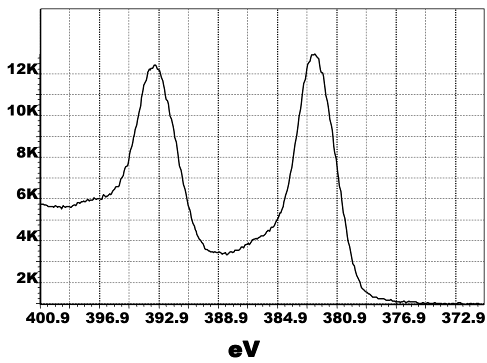

Figure 3.9: Sample 1 U4f Peaks

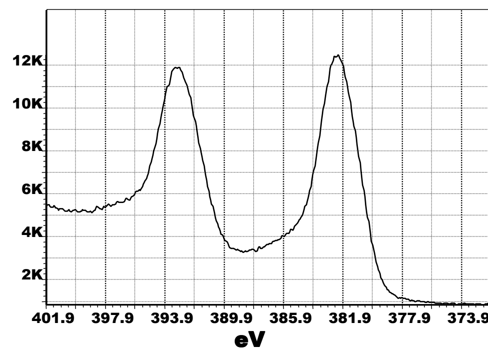

Figure 3.10: Sample 2 U4f Peaks

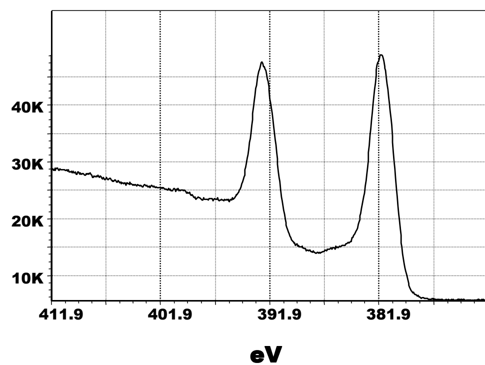

Figure 3.11: Sample 2 after 13 Weeks

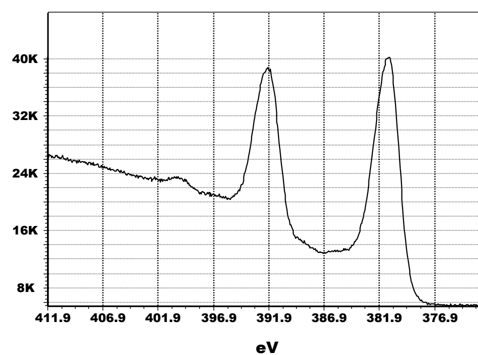

Figure 3.12: Sample 1 after 18 Weeks

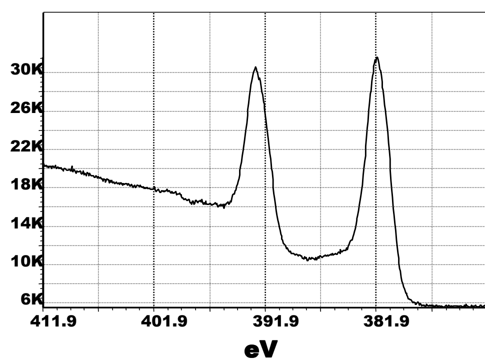

Figure 3.13: Sample 2 after 25 Weeks

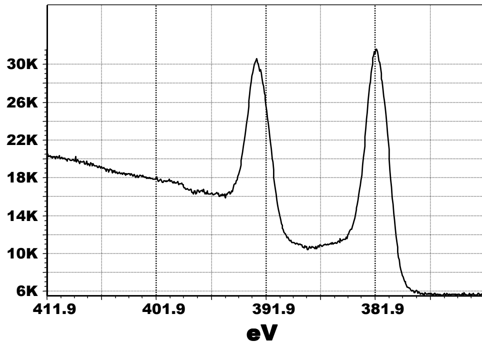

Figure 3.14: Sample 2 after 25 Weeks Incident Angle=55

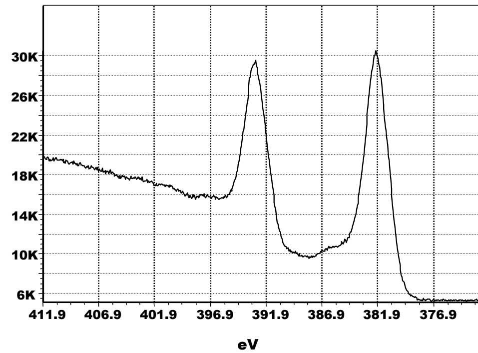

Figure 3.15: Sample 2 after 25 Weeks Incident Angle=75

different incident angles, the uranium $4f_{5/2}$ and $4f_{7/2}$ peaks were also examined with an angle of 75 degrees. One can see from Figures 3.14 and 3.15 that with a greater incident angle, the uranium peaks shift to slightly higher energies. This is because we were able to sample more of the top layer with a larger incident angle, showing a higher oxidation state in the top layer than further down in the sample.

3.3.4 Sampling Depth

The depth from which XPS data is compiled depends on two factors: the kinetic energy of the electron and the x-ray incidence angle, θ. An electron with greater kinetic energy can travel through more material before undergoing inelastic scattering and losing its energy. Hence, electrons with less binding energy (and more kinetic energy) come from deeper within the sample. As can be seen qualitatively from Figure 3.16, the sampling depth is also a function of the incidence angle. X-rays travelling at a smaller angle with respect to the normal of the sample will penetrate deeper before encountering an electron and thus the sampling depth will be greater.

The kinetic energy for the oxygen 1s electrons is approximately 570 eV and of the uranium 4f electrons is 720 eV. The difference in sampling depth was determined to be about 5 Å. Hence, the oxygen 1s peaks show the oxidation of the

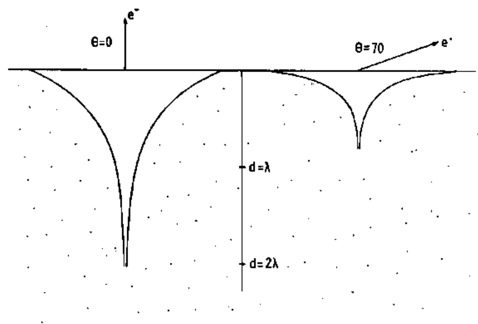

Figure 3.16: Depth Profile with Angle [38]

surface, while the uranium 4f peaks show the oxidation behavior of the layers just below the surface, and it is obvious that the two trends are not similar. The scans run at various angles are in agreement with what was determined by the uranium 4f and oxygen 1s peaks. The scan done at 55 degrees (which samples a greater depth) shows a slightly lower oxidation state than the scan done at 75 degrees.

3.3.5 Composition of Samples

All of the samples, except sample UO16, that we used for determining optical constants were measured using XPS two days before reflection measurements were taken at the Advanced Light Source (ALS) Synchrotron at Lawrence Berkeley National Labs. The samples were made over a four day period, excluding sample UO11 which was made 4 days before any others, but the composition of the top layer of each sample appeared to be very similar. From the graphs of the uranium $4f_{5/2}$ and $4f_{7/2}$ peaks and the graphs of the oxygen 1s peak, it is apparent that samples UO12 through UO15 are very similar in composition to the depth measurable by XPS (about 15 Å).

Sample UO11 appears to be of slightly different composition than the other samples. In comparison with Figure 3.3 [35], the top layer of samples UO12–UO15 seems to be U_2O_5, with a binding energy of 381.9 eV, while that of sample UO11 appears to be U_3O_8, with a binding energy of 382.1 eV. Sample UO11 was the first

sample made in the group and was also the thinnest of the five, approximately 50 Å of uranium oxide deposited on a silicon wafer. Thus, it would make sense for the top layer of that sample to be slightly more oxidized than the other samples.

From previous studies we performed, it appeared that although the films were initially UO_2, or very close to that composition, the top layer rapidly oxidized to higher valence states and ultimately to UO_3. These samples had not quite oxidized to UO_3 at the time of measurement, as it seems to take several weeks. Thus, the samples we measured at the ALS had a small layer of an unknown uranium oxide on top of UO_2.

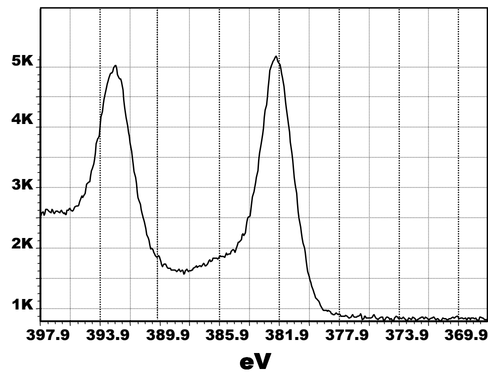

Figure 3.17: XPS for Sample UO11

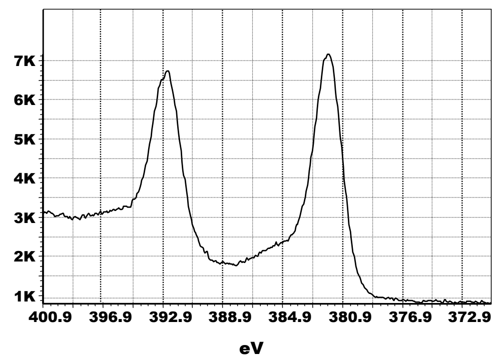

Figure 3.18: XPS for Sample UO12

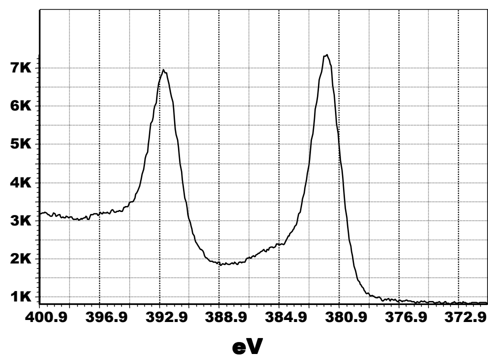

Figure 3.19: XPS for Sample UO13

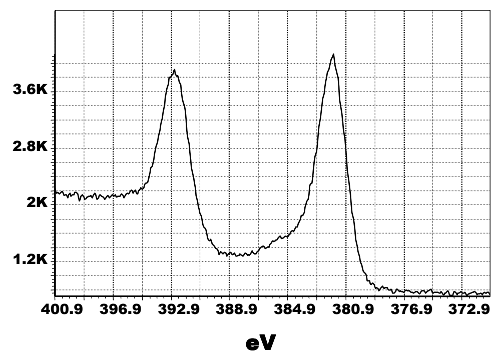

Figure 3.20: XPS for Sample UO14

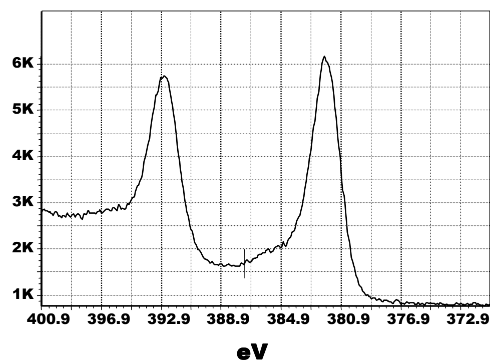

Figure 3.21: XPS for Sample UO15

3.4 Atomic Force Microscopy (AFM)

Once composition and thickness of the samples was determined, AFM was used to determine the roughness of our samples. This information is necessary for ellipsometry and reflectance modelling of the samples.

Guillermo Acosta, a member of our research group, made it possible for us to get thickness information using AFM. When the substrate was placed on the sample holder before deposition, a razor blade, called an abrupter, was placed at an angle on a corner of the substrate. The razor blade masked a portion of the substrate during deposition, creating an abrupt edge between the deposited film and the substrate. AFM can measure the difference in heights on either side of the edge and give another measurement of sample thickness. So far, relatively good agreement has been found between thicknesses calculated using XRD and this technique in AFM. Figure 3.22 shows an AFM image of the abrupt edge on sample UO13, which was measured by XRD to be 185 Å of UO_2. From AFM, this sample appears to be 240 Å thick. Other measurements using AFM gave values closer to that obtained by XRD but the picture was less clear. The abrupter could cause the sample to be thicker right on the edge of the film due to buildup of the film against the razor blade during deposition. The usefulness of this technique requires further study.

There are two types of roughness for a film, extrinsic and intrinsic. Extrinsic is the roughness from the substrate on which the film was deposited while intrinsic is the roughness at the top of the film due to deposition technique. It is important to understand both types of roughness to truly characterize our films. Before our set of samples was made, we measured one silicon wafer from the set using AFM to determine its RMS roughness. This was determined to be approximately 2 Å across a 1 μm area. The RMS roughness of sample UO12 was measured to be about 3 Å across a 1 μm range, as shown in Figure 3.23. All of the samples were

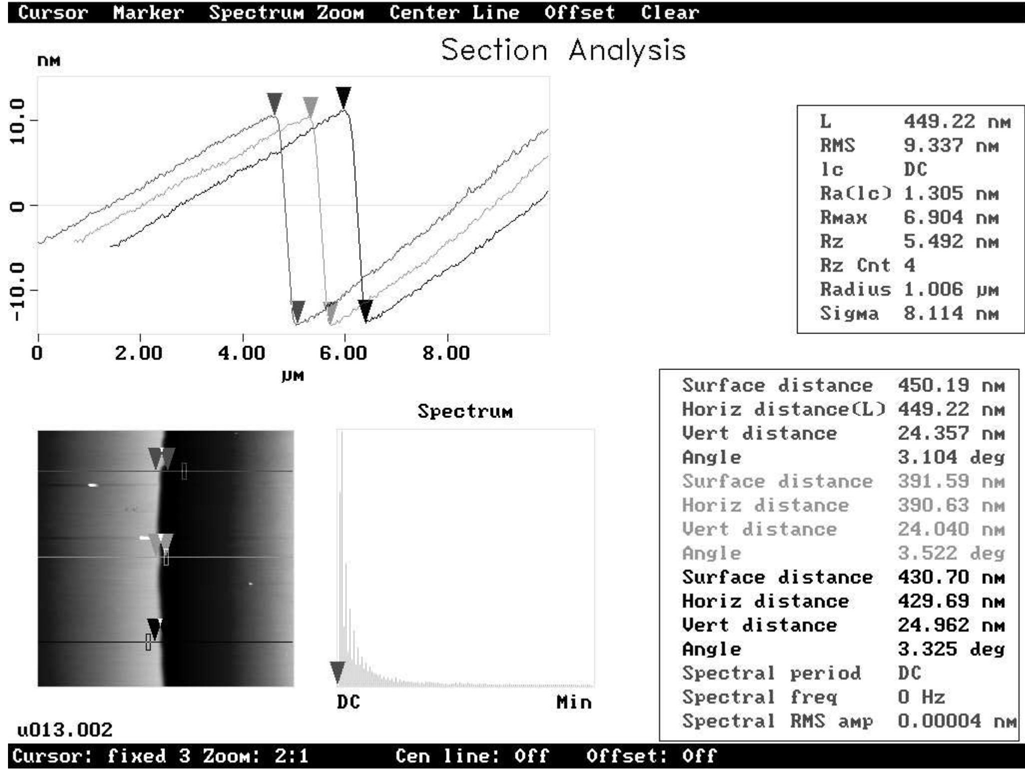

Figure 3.22: Thickness of Uranium Samples from AFM

assumed to have similar roughness since we were unable to do AFM on all of the samples.

The effect extrinsic roughness has on the surface of the deposited film depends on the thickness of the film. For thick samples, the extrinsic roughness is smoothed out and only intrinsic roughness affects the surface roughness. For thin samples, though, the surface roughness of the film will be a combination of intrinsic and extrinsic roughness. If intrinsic roughness is represented by $h(x)$, extrinsic roughness is represented by $f(x)$, and $a(x)$ is the fraction of the roughness from below that propagates, the extrinsic roughness for each layer can be represented by

$$f_i(x) = h_i(x) + a_i(x)(f_{i-1}(x)) \ . \tag{3.4}$$

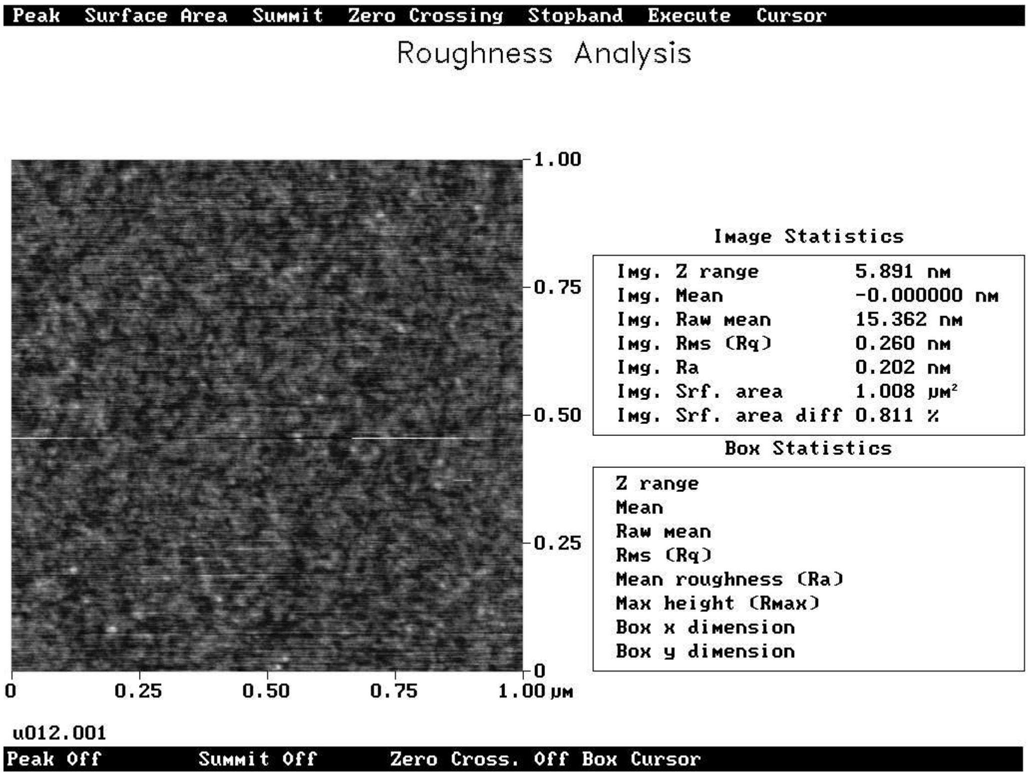

Figure 3.23: Roughness of Uranium Samples from AFM

A further description of the effect of roughness on optical properties can be found in Stearn [39].

Chapter 4

Reflectance

4.1 BYU Data Acquisition

We used a monochromator at BYU that can measure the reflectance of films versus angle in the range desired. The McPherson, Model 225, 1-meter scanning monochromator can measure reflectances in the range from 1200 Å to about 300 Å using a hollow cathode DC continuous line source and a 1200 lines/mm reflective grating.

Figure 4.1 shows the McPherson monochromator with the octagonal measurement chamber. The measurement chamber used with the McPherson monochromator has a sample stage and detector mount that move in theta [40]. This allows reflectance measurements to be taken from grazing angles of 2.5° to 80° incident to the mirror. Difficulties with this system are that if the alignment is off by a small amount, the measurements at small angles are not accurate as much of the beam misses the detector. For example, if the x position of the mirror is off by 0.1 mm at a mirror angle of 2.5°, the beam will be shifted horizontally by 2.29 mm. Since the hole on the detector is only 3 mm in diameter, this means that a misalignment in the x direction could cause the main part of the beam to miss the detector, resulting in fewer counts being recorded at that angle. Examples of data showing good and bad alignment are shown in Figures 4.2 and 4.3.

Alignment is performed using a laser that was previously aligned to the diffraction grating and slits of the monochromator. Details on alignment can be

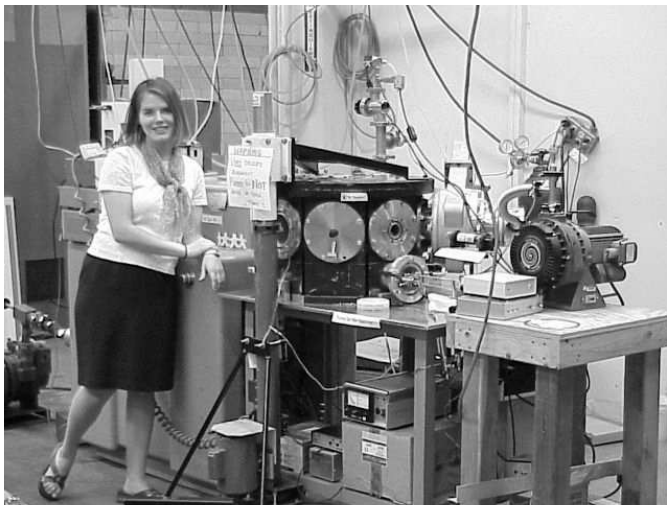

Figure 4.1: McPherson Monochromator and O-chamber

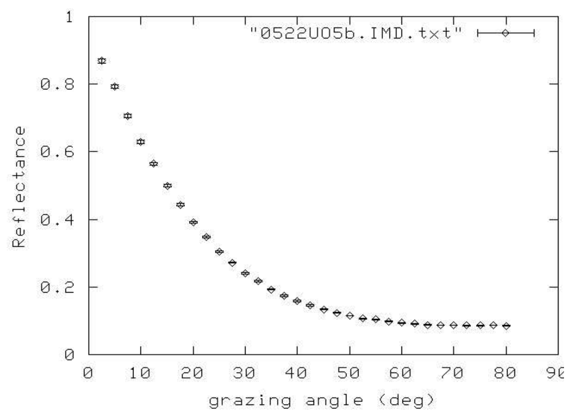

Figure 4.2: Perfect Alignment

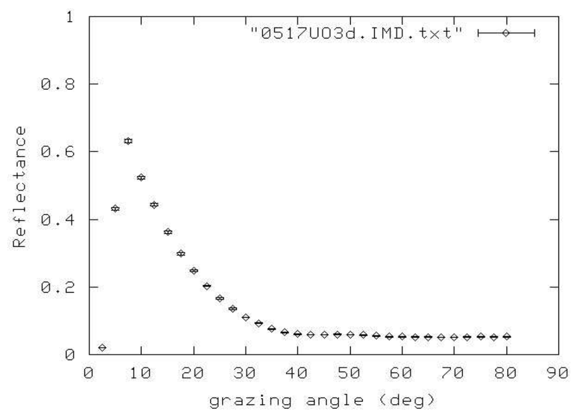

Figure 4.3: Poor Alignment

found in Squires [40]. Samples of uranium oxide thickness from 25 Å to 250 Å were measured in this chamber at wavelengths of 304 Å, 537 Å, and 584 Å using He gas.

The detector used in this system was an MD-501 AMPTEKTRON channel electron multiplier (CEM). To avoid damaging the CEM, the measurement chamber that contains the detector must be at pressures below 2×10^{-5} torr before the detector is turned on. Background noise, measured with the detector on but no EUV light reaching it, was about 1 count/half second.

4.2 BYU Data

After measuring the samples using the McPherson monochromator, the reflectance versus grazing angle data was read into IMD. A model of the sample was built using optical constants for UO_2 obtained theoretically from literature [17, 41, 42]. The constants used at 304 Å were δ=0.40343 and β=0.426760 and calculated from the theoretical atomic scattering factors [17]. The constants at 584 Å were a bit more difficult to find. From previous work at BYU, Squires reported a value of δ=0.41 for U at 584 Å [41]. From Fäldt [42], one can read off a graph the values for U of ϵ_1 and ϵ_2 and calculate n and k. The values are: ϵ_1=3, ϵ_2=1.5, n=1.782, and k=0.42077. Since no data exists at 584 Å for UO_2, the values obtained from U were used in the model. The optical constants used to build the model are only a starting point in fitting the measured data so only needed to be approximate.

After the model was built and the measured data read into IMD, a fit of n and k were performed at a fixed wavelength. IMD had difficulties fitting the data well with just a UO_2 layer. As a result, I wrote a program in MATLAB that fit the optical constants of UO_2 as well as those of the top oxide layer. The optical constants calculated for UO_2 with an oxide of 18 Å on top from the data obtained at BYU is shown in Table 4.1 and the constants for the top oxide are shown in Table 4.2. The error bars are the average of the difference of the constants obtained using oxide thickness of 20 Å and 15.5 Å. From the table, one can see

Table 4.1: Optical Constants for UO_2 from BYU Data

	Measured		**Calculated from f_1 and f_2 [17]**	
λ in Å	δ	β	δ	β
304	-.0069±0.0026	.0896±0.0034	0.40343	0.426760
537	.2107±0.0023	.4794±0.0015	-	-
584	.5179±0.0028	.5472±0.0076	-	-

Table 4.2: Optical Constants for Top Oxide from BYU Data

	Oxide Layer Measured	
λ in Å	δ	β
304	.5380±0.0585	.4495±0.0242
537	-.1679±0.0354	.5883±0.0175
584	-.6251±0.0918	.7485±0.0363

that the top oxide constants are strongly dependant on the thickness of the layer. The calculated constants were obtained from measurements of μ, the atomic photoabsorption crosssection, used to obtain f_2 and f_1 obtained by Kramers-Kronig relations. It is interesting to note the similarities between the constants for UO_2 at 304 Å calculated from atomic scattering factors and the measured constants for the top oxide at that wavelength. The samples were put into the measurement chamber attached to the monochromator within a few minutes of removal from vacuum and were kept under vacuum throughout the measurements at the different wavelengths. To increase the number of counts detected by the channeltron at the lower wavelengths, the counting time was increased from 0.5 seconds at 584 Å to 1.5 seconds at 537 Å to 2 seconds at 584 Å. This meant that a full measurement of reflectance versus angle for a sample at 304 Å took an hour.

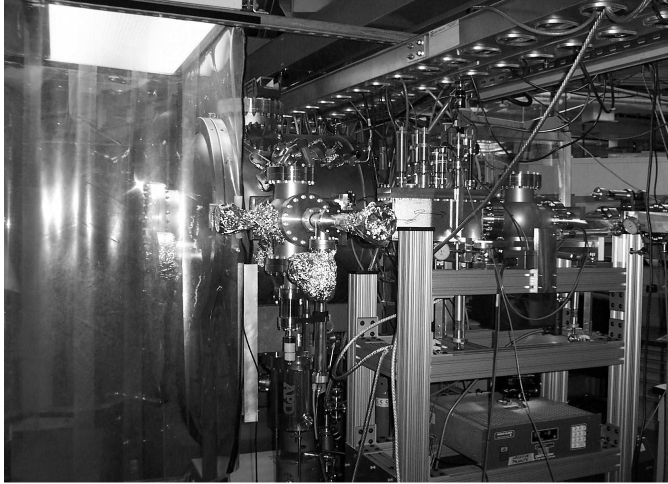

Figure 4.4: Reflectometer at the ALS

4.3 ALS Data Acquisition

All measurements at wavelengths below 304 Å were done at the Advanced Light Source (ALS) synchrotron at Lawrence Berkeley National Laboratory in California. These measurements were performed using beamline 6.3.2 on which there is a reflectometer for reflectance measurements of samples. A picture of the reflectometer is shown in Figure 4.4 and a view of the synchrotron ring is shown in Figure 4.5. Measurements can be taken at energies from 50 to 1300 eV and at various angles. Detailed descriptions of synchrotron radiation and applications of this radiation can be found in Attwood [1] and through links on the CXRO web page [43]. A description of beamline 6.3.2 can be found in Underwood [44].

Beamline 6.3.2 has three gratings that allow measurements to be taken from 50 to 1300 eV: 200 lines/mm, 600 lines/mm, and 1200 lines/mm. Only the 600 lines/mm and 1200 lines/mm gratings were used to reach the desired range of 24 Å to 400 Å. Different filters are used with each grating to select the specific wavelength desired. As can be seen from Figure 4.6, data taken at the same wavelength using different filters is not exactly the same. This is due to some of

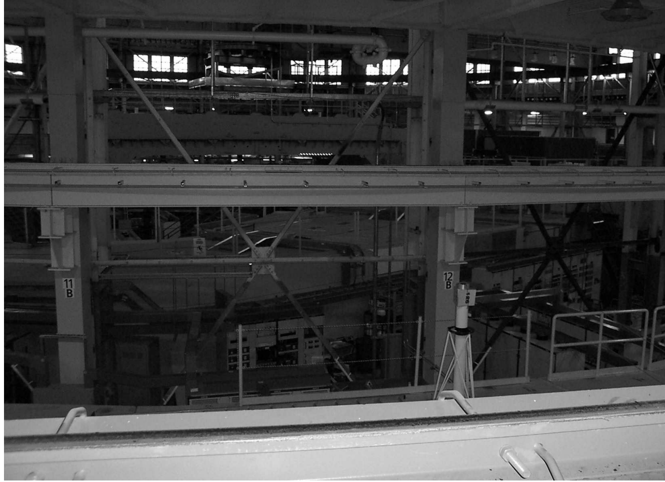

Figure 4.5: View of the Synchrotron Ring at the ALS

the filters allowing orders other than the desired order through, causing the source to be slightly nonmonochromatic.

For each wavelength range, data was taken with the sample out of the way of the beam to get the I_0 measurement. Also, the background was measured by blocking the source entering the monochromator and taking data with the photodiode. The dark data, as we called the background, was on the order of 1×10^{-4}. As it was so low, we did not need to subtract the background from the reflection data. The reflection data was taken over a range of angles. Data was stored as follows: the diode response in counts, m3 or the current in mirror m3, and the beam current in mA. Reflectance was calculated as

$$R = \frac{I_{\text{diode}}}{I_{\text{zdiode}}} \frac{I_{\text{zm3}}}{I_{\text{m3}}} \ , \tag{4.1}$$

where I_{zdiode} is the I_0 diode response and I_{zm3} is the current in the m3 mirror for the I_0 run. The stability of the values for m3 and the source current were compared and found to be approximately the same, thus it was purely choice in deciding whether to normalize the reflectance data by m3 or by the beam current.

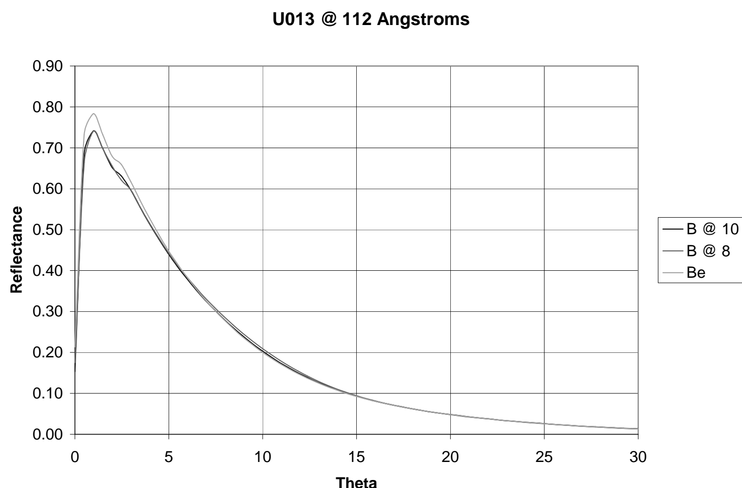

Figure 4.6: Reflection Data using Different Filters

4.4 ALS Data

Data taken at the ALS was analyzed using MATLAB. The code for the programs can found in Appendix 5. The MATLAB code was checked against IMD and calculations performed on the CXRO web page [17] and they all agreed exactly. The structure of the film used in the analysis was the same as in Figure 1.3 with perfectly abrupt boundaries and no roughness. Roughness was not used in this study as the few Å's of roughness present on our samples did not affect the reflection of the samples when checked in IMD. As stated in Section 3.4, the roughness of the substrate was on the order of 2 Å while the roughness of the total film was about 3 Å.

The measured reflectance of each sample was calculated at 9 wavelengths between 45 Å and 175 Å. The thickness of the top oxide was determined by fitting its thickness, without including the change in density, using data from all six samples and fitting at each wavelength of interest. The reasonable thickness values obtained in this manner, from 44–55 Å, were averaged to get 50 Å. This value was fixed for the thickness of the top oxide in all subsequent fits. A fit was then

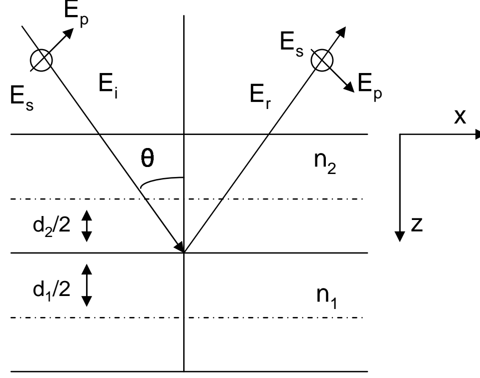

Figure 4.7: Geometry for Reflection Calculations

performed using data from all six samples to determine the δ and β for the UO_2 layer and for the top layer of unknown oxide.

To calculate the theoretical reflectance of our films after a fit of the optical constants was performed, we used the Fresnel coefficients, r_s and r_p. From Kohn [45] and Parratt [46], the Parratt recursion formulas allow calculation of the Fresnel coefficients for a bilayer. The following equations were used in the MATLAB code contained in Appendix 5 for analysis of our films and determination of theoretical reflectance:

$$Sq_2 = \sqrt{n_2^2 - (\cos(\theta))^2} \tag{4.2}$$

$$k_{z2} = kSq_2 \ , \tag{4.3}$$

with the wave number defined as $k = \frac{2\pi}{\lambda}$. C_2 includes the phase information for the wave calculated halfway between the layers as in Figure 4.7:

$$C_2 = e^{ik_{z2}D_2/2} \ . \tag{4.4}$$

The equations for f_s and f_p are variations on the Fresnel coefficient equation:

$$f_{s2} = \frac{Sq_2 - Sq_1}{Sq_1 + Sq_2} \tag{4.5}$$

$$f_{p2} = \frac{n_1^2 Sq_2 - n_2^2 Sq_1}{n_1^2 Sq_2 + n_2^2 Sq_1} \tag{4.6}$$

These are then used to calculate the recursive Fresnel coefficients r_s and r_p:

$$r_{s2} = C_2^4 \frac{f_{s2} + r_{s1}}{1 + f_{s2} r_{s1}} \tag{4.7}$$

$$r_{p2} = C_2^4 \frac{f_{p2} + r_{p1}}{1 + f_{p2} r_{p1}} \ . \tag{4.8}$$

The actual reflectance for the sample is calculated using the coefficients for the Nth layer, R_s and R_p:

$$R_s = |r_{sN}|^2 \tag{4.9}$$

$$R_p = |r_{pN}|^2 \ . \tag{4.10}$$

The actual reflectance is $R_s = RC^2$ but for the top layer $C = 1$. Therefore, the total reflectance of the film is found by combining R_s and R_p according to the polarization of the source. At the ALS, the source was 90% s-polarized so $R = .1R_p + .9R_s$.

Errors for the indices of refraction were calculated in the following manner. Systematic errors were evident in most of the reflection versus angle scans as the reflection at low grazing angles did not go to one. This was due to misalignment in the z-direction and seemed to be most evident below 2°. Therefore, the data below this point was cut off before the fit was performed.

Statistical errors were determined by comparing the χ^2 for the fit. The data was fit in MATLAB using fminsearch to minimize the function s:

$$\begin{aligned} s_1 &= \sum (R_m - R_{c1})^2 \\ &\vdots \\ s_N &= \sum (R_m - R_{cN})^2 \\ s &= s_1 + \cdots + s_N \ , \end{aligned} \tag{4.11}$$

where N is the number of samples used in the fit, R_m is the measured reflectance, and R_{ci} is the calculated reflectance for sample i. The outputs of this fit are the optical constants of the UO_2 layer and of the top oxide.

To calculate the statistical errors in the fit and to put error bars on the resulting optical constants, χ^2 was calculated and fit. First, the standard deviation of the calculated data from the measured data was calculated as

$$\sigma^2 = \frac{s}{F} \ , \tag{4.12}$$

with $F = N - p$, F being the degrees of freedom, N the number of data points, and p the number of fit parameters. Then χ^2 is evaluated as

$$\chi^2 = \frac{s}{\sigma^2} \ . \tag{4.13}$$

For the initial χ^2 in the fit, the value used for s, called s_0, was from the fit of all four optical constants. Then χ^2 becomes

$$\chi_0^2 = F \ . \tag{4.14}$$

Three of the optical constants were then fixed at their fit values and the remaining constant was fit. This s was then used to evaluate χ^2 using the value for σ calculated as in Equation 4.12 with s replaced by s_0. The function

$$f = (\chi^2 - \chi_0^2 - 1)^2 \tag{4.15}$$

was then minimized. This tells us how much the index we are fitting can change to cause χ^2 to be greater than χ_0^2 by one. The function is squared because of the use of a minimum finder. Values for f were typically on the order of 1×10^{-5}.

The optical constants obtained for UO_2 can be found in Figures 4.8 and 4.9 and in Table 4.3. The optical constants for the top oxide layer can be found in Figures 4.10 and 4.11 and in Table 4.4. The dip in δ at 125 Å for UO_2 seems to coincide with a resonance and appears to follow structure found in theoretical calculations.

We were able to measure reflection of sample UO13 at the ALS at 300 Å in order to compare it with data taken with the McPherson monochromator at BYU. The reflection curves are shown in Figure 4.12. From the figure, one can see that

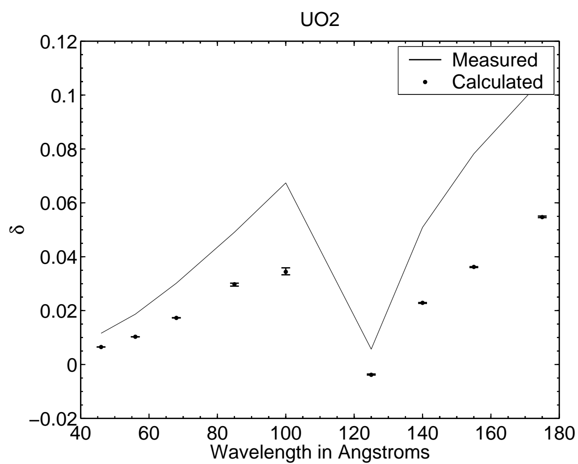

Figure 4.8: UO_2 δ

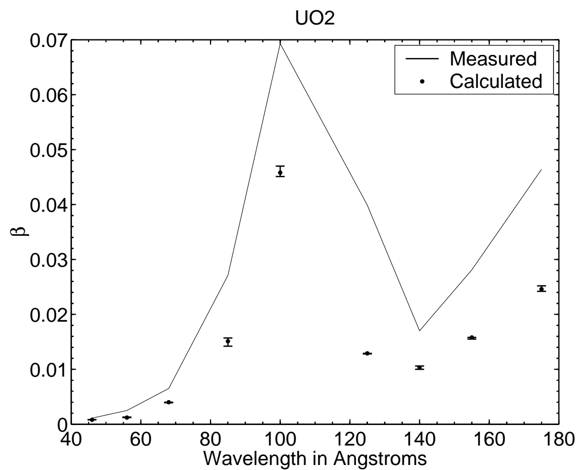

Figure 4.9: UO_2 β

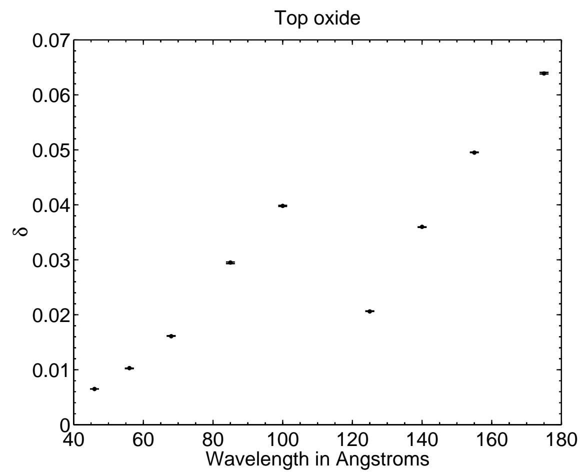

Figure 4.10: Top Oxide Layer δ

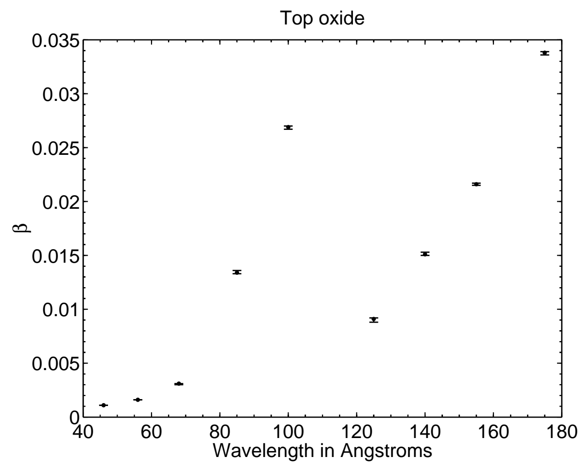

Figure 4.11: Top Oxide Layer β

Table 4.3: Optical Constants for UO_2

	Measured		**Calculated(f_1&f_2) [17]**		$\frac{\delta_M}{\delta_C}$	$\frac{\beta_M}{\beta_C}$
λ in Å	δ	β	δ	β		
46	.0065±0	8.0861e-4±0	.0116	.0011	0.56	0.74
56	.0103±0	.0012±.0001	.0187	.0025	0.55	0.48
68	.0173±.0001	.0040±.0001	.0302	.0065	0.57	0.62
85	.0298±.0005	.0151±.0007	.0491	.0271	0.61	0.56
100	.0344±.0011	.0458±.0011	.0674	.0693	0.51	0.66
125	-.0038±.0002	.0129±.0001	.0057	.0399	-	0.32
140	.0229±.0002	.0103±.0003	.0509	.0170	0.45	0.61
155	.0362±.0002	.0158±.0002	.0782	.0281	0.46	0.56
175	.0547±.0003	.0246±.0005	.1058	.0464	0.52	0.53

Table 4.4: Optical Constants for Top Oxide Layer

	Measured	
λ in Å	δ	β
46	.0065±0	.0011±0
56	.0103±.0001	.0016±0
68	.0161±.0001	.0031±.0001
85	.0295±.0002	.0134±.0001
100	.0398±.0001	.0269±.0002
125	.0206±.0001	.0091±.0002
140	.0360±.0001	.0151±.0001
155	.0495±.0001	.0216±.0001
175	.0639±.0002	.0338±.0002

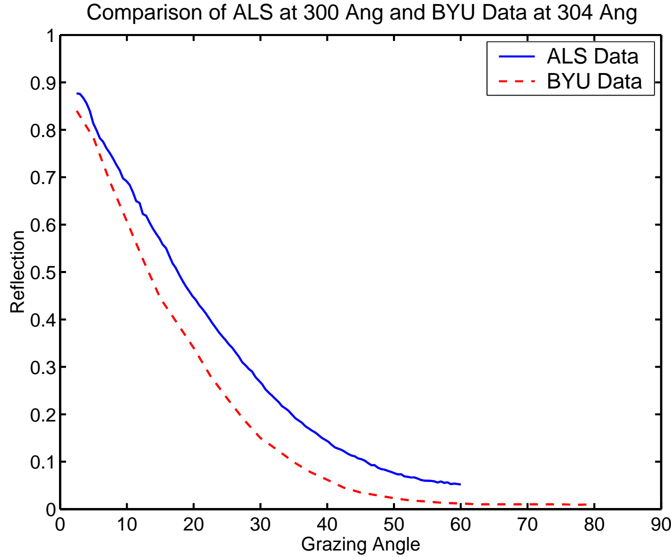

Figure 4.12: Comparison of Reflection Measurements at the ALS at 300 Å and at BYU at 304 Å

the ALS data gives a much higher reflection than the BYU data. The ALS optimal measurement range is well below 300 Å. At the longer wavelengths, the filters are less effective at cutting out higher orders so the reflection could be higher due to multiple orders adding.

4.5 Data Analysis

The theoretical constants were calculated from atomic scattering factors from the CXRO web site [17] using a density of 10.96 g/cm^3 for the density of UO_2. The theoretical δ and β for UO_2 appear to be much greater than the measured values. This would mean that theoretically, UO_2 is less reflecting and more absorbing than it is measured to be. This is one reason that it is vital to know the optical constants of a material in designing multilayer mirrors in the EUV.

From a comparison of the measured and theoretical constants, it appeared that the difference could be due to a difference in density between the measured films and the calculated density of UO_2. This is because the measured δ and β for

UO_2 are much smaller than the theoretical values. To test this hypothesis, studies were done using ellipsometric and XRD data.

All six of the samples were measured using ellipsometry shortly after sputtering. Initially, the model used did not include the top oxide. The thicknesses of the samples were set at those values obtained from XRD. Initial values for the optical constants were obtained from previous fits on UO_x samples. A point-by-point fit was performed on n and k and new constants were obtained. The two thinnest samples, UO11 and UO16, had similar constants but they were much different than the other samples.

Studies were also performed of how the n and k of sample UO12 were fit to see how model dependant the fit was. First, the fit was performed of n and k at the same time using initial values obtained from sample UO15. Then, k was fixed at the values from UO15 and n was fit. This was repeated for k with n fixed. A summary of the results can be found in Table 4.5. This study is not very clear as

Table 4.5: Study of n and k from Ellipsometry

Source	eV	n	k
Schoenes [13]	5.12	2.7155	0.4223
	4.24	2.3685	0.1509
	2.38	2.3459	0.3141
UO12 fit n and k	5.12	0.45543	0.92181
	4.24	0.6688	1.2971
	2.38	1.7842	0.98429
UO12 fit n	5.12	2.1151	0.47337
	4.24	2.2342	0.36821
	2.38	1.992	0
UO12 fit k	5.12	2.0283	0.43998
	4.24	2.2327	0.40681
	2.38	2.0727	0.53288

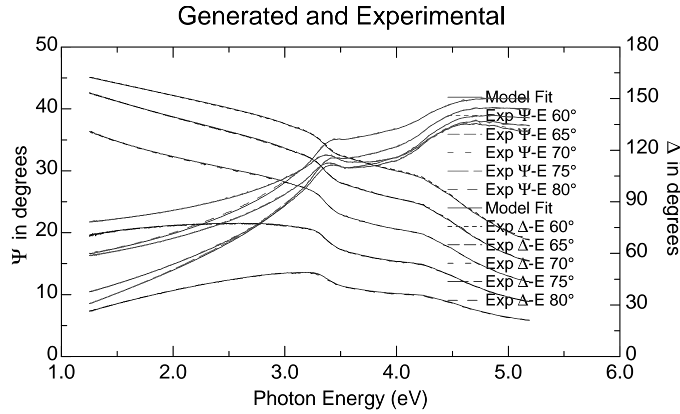

Figure 4.13: Fit for UO13 of Ψ and Δ with an Oxide on top, MSE=2.7449

vastly different values for n and k were obtained when fitting both of the constants or just fitting one. From this it seems that ellipsometric fits are very dependent on the model and on the initial conditions. An example of a fit performed using ellipsometry is shown in Figure 4.13.

Since the ellipsometric data is obtained in air, the samples were able to oxidize so another fit was performed using an oxide on top of the UO_2. The constants for the top oxide were those obtained from UO16 since it is the thinnest sample, 35 Å, and would completely oxidize within a few minutes. The initial values for the constants of the UO_2 layer were those obtained for sample UO15 in the above fit. First, the thicknesses of the UO_2 and oxide layers were fit. The results were reasonable with the values obtained shown in Table 4.6 where T_0 is the thickness of the film determined by XRD. Sample UO16 was not included in the table because its constants were used for the top oxide layer and it was assumed to be fully oxidized. Constants obtained from these fits and their comparison with values from literature are found in Figures 4.14 and 4.15.

Using the thicknesses from the fit, n and k were fit. Not surprisingly, sample UO11 at 50 Å was found to be completely oxidized. The fit for the thicker samples did not change much with an oxide layer on top and some of the fits wanted a thickness of zero for the top layer. This could be because the samples were

Table 4.6: Thickness Fit from Ellipsometry

Sample	T_0 (Å)	UO_2 T (Å)	Oxide T (Å)	MSE
UO11	50	0	50	1.161
UO12	110	108	0	10.791
UO13	185	183	0	2.7976
UO14	225	225	4.95	19.587
UO15	250	250	5	26.54

measured within minutes of removal from the sputter system. In the fits for samples UO12–UO15, the values of k were similar to those reported by Schoenes [13]. The values of n from the fit for these samples were also similar to Schoenes's values. This is a different trend to that found in the ALS and monochromator data. These differences could be because Schoenes determined his values from experiment and not from atomic scattering factors. Thus, the discrepancy between the measured data and atomic scattering data does not appear to be due to any density differences between the films and UO_2.

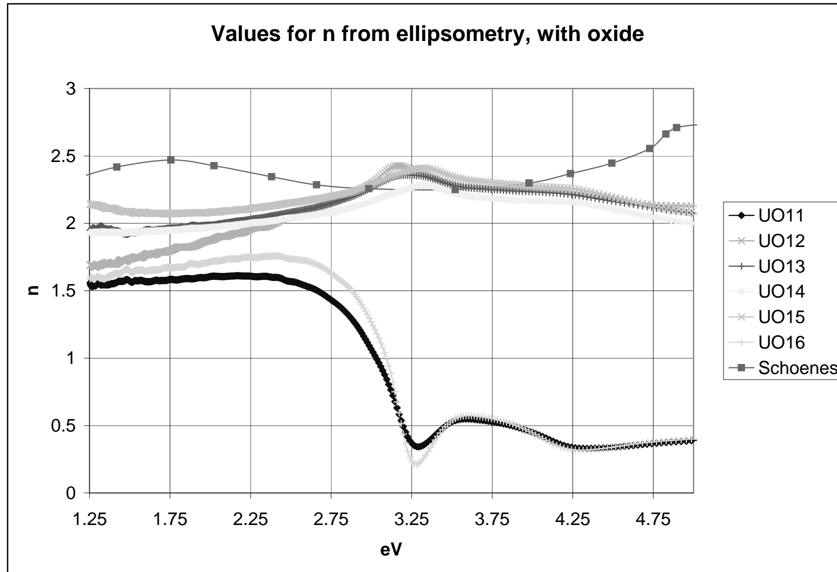

Figure 4.14: Values for n from Ellipsometry

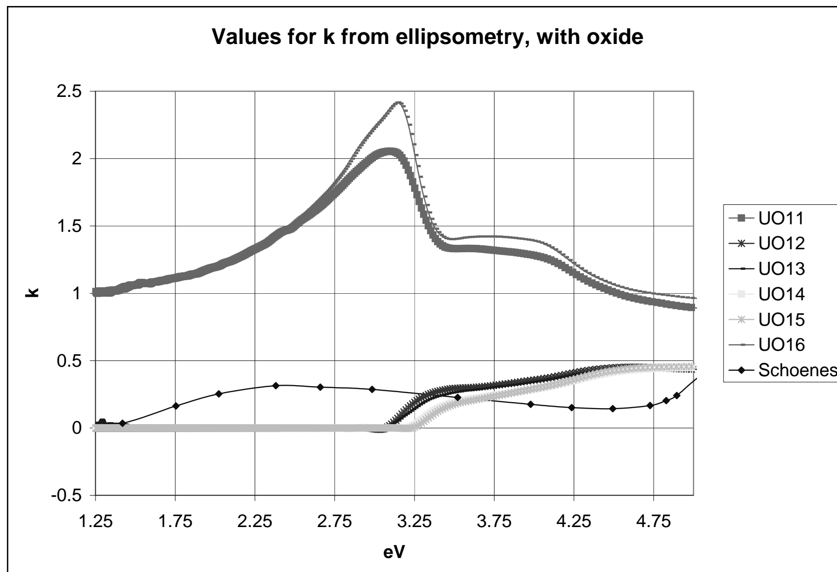

Figure 4.15: Values for k from Ellipsometry

Table 4.7: Fit of XRD Data for Sample UO12

Fit	UO_2 Thickness	Normalization	Angle Offset	ρ
ρ fixed	107.0±0.3	57±2	-0.062±0.003	1
vary ρ only	107.0	57.0	-0.062	0.99±0.01
vary all	109.7±0.4	161±11	0.001±0.003	0.54±0.02

Through further XRD studies, we were able to better fit the data by allowing various parameters to change. First, the data had to be normalized and this was used as a fit parameter. Also, the angle alignment could be slightly off so an angle offset was included in the fit. Since the focus of this study was to determine if the density of our films was different than UO_2, the density was also allowed to change. Results from various fits of these values, as well as the thickness of the UO_2 layer are shown in Table 4.7 where ρ is the density of the film. Allowing all parameters to vary reduced the mean square error by about two. Figure 4.16 shows the data from XRD and the values from these three fits.

The XRD data for sample UO13 was a bit more difficult to fit because at the low angles we were very close to the critical angle. Since the measurements for UO12 and UO13 should have been made with the same angle offset, we tried fitting the data for UO13 using the values from sample UO12 and allowing only the thickness to vary. Under these conditions, it got the nominal thickness of 185±1 with a fixed ρ of 1.0. If we let ρ float, the thickness is 180±1 and $\rho = 0.79 \pm 0.03$. These fits are shown in Figure 4.17.

XRD studies were unable to conclusively show any differences in the density of the films from UO_2 but they did confirm the film thicknesses previously determined.

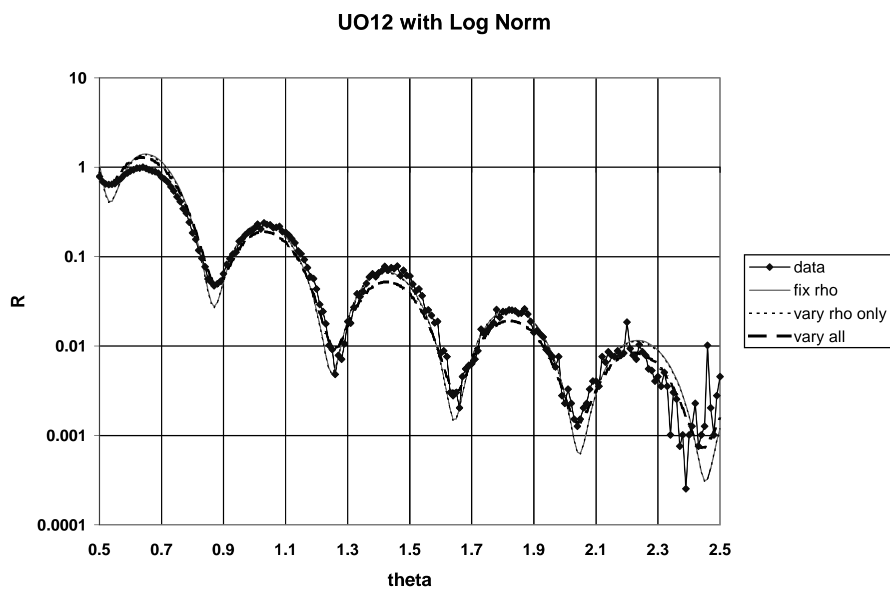

Figure 4.16: XRD Fit for Sample UO12

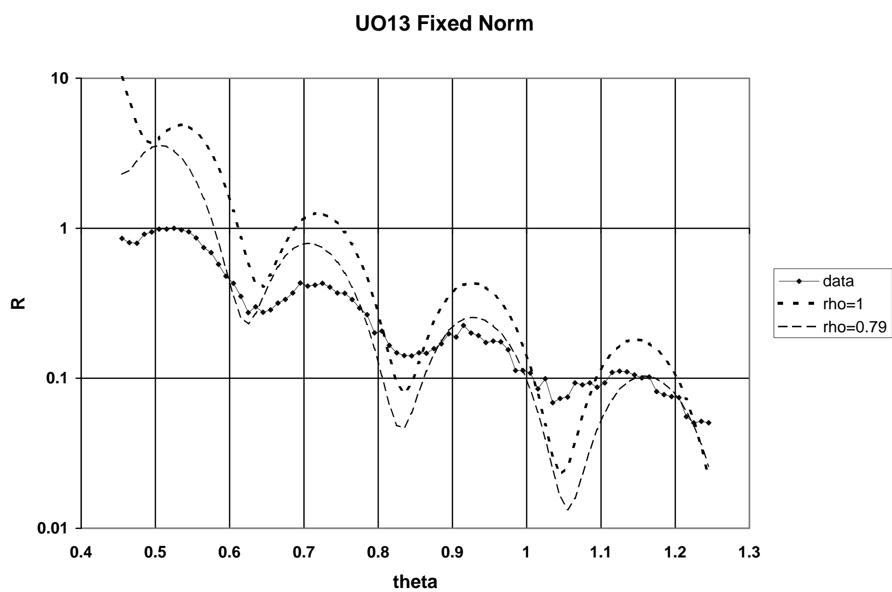

Figure 4.17: XRD Fit for Sample UO13

Chapter 5

Conclusion

This study on the optical constants of UO_2 has resulted in some interesting findings. First, it was discovered that while UO_2 forms on pure uranium metal at room temperature in atmosphere and seems to stabilize over time, the film will continue to oxidize until it is all UO_3. Thus, the oxide that formed on top of the UO_2 films had to be taken into account in fitting for the optical constants. Second, reactive sputtering of uranium in an oxygen atmosphere will produce films of the oxide composition desired if sputter rates in relation to the oxygen partial pressure are known. Third, the optical constants obtained in this study for reactively sputtered thin film UO_2 vastly differ from theoretical constants calculated by CXRO [17]. No experimental values for the optical constants of UO_2 in the full range from 46 Å to 175 Å have been previously reported so the measured data can only be compared to theoretical calculations in this region. These results show that the theory of optical constants in the EUV is still not fully understood.

Due to time constraints, the data obtained at the ALS on these films has not been fully analyzed. Over 300 data files were generated and require further study. Only the data taken at the same wavelength for each sample was studied to be able to fit the optical constants across the samples.

Differences in the measured optical constants of UO_2 and those obtained from atomic scattering factors could be due to several factors. First, differences in density between the films studied and the reported density of 10.96 g/cm^3 for

UO_2 could account for the low δ and β in the measured data if they were off by the same ratios at all energies. We studied this effect using ellipsometry and XRD. The XRD data proved to be fairly independent of density. The ellipsometric data seemed to show that the density of our films were at least similar to the density of the films used by Schoenes [13]. Thus, it appears that the differences in the constants are not entirely due to density affects. The differences could also be due to the atomic scattering factor theory not begin completely accurate in the EUV where electrons are still bound and especially at resonances.

The Weaver [8] data was calculated from μ from transmission data from experiments done by Weaver and Fäldt [42]. The reported values from Fäldt seem to be either extrapolated from his data or read from the plot so may not be that accurate. Henke [9] stated that the atomic scattering factors were calculated from experimental values of μ if available or if no data was available, a best-fit f_2 curve was obtained by interpolation or extrapolation through Z. Chantler [10] stated that the previous calculations of the atomic scattering factors from μ had severe limitations so the main focus of these tables are to fix the dispersion relations to determine f_2.

Appendix A

Included here is the MATLAB code The main file is fitrefl.m which calls the files to calculate the measured reflection of the samples and fits the optical constants. The code for fitrefl.m is as follows:

```
clear; close all;
%This file will fit the measured and experimental data to get
%delta and beta.
%It will call calcrefl through leastsq.m to calculate
%reflection each time we fit.
%It will call reflmeas to compare to measured reflection.

%Calculate reflection, measured reflection, compare, if
%within limit end.
%Spit out delta and beta.
lambda=input('Enter wavelength in angstroms - ');

%This is to calculate the measured data at one wavelength
%for all samples
sample=input('Enter sample name - ', 's');
[Rm1,angle1]=reflmeas(sample,lambda);
sample=input('Enter sample name - ', 's');
[Rm2,angle2]=reflmeas(sample,lambda);
sample=input('Enter sample name - ', 's');
[Rm3,angle3]=reflmeas(sample,lambda);
sample=input('Enter sample name - ', 's');
[Rm4,angle4]=reflmeas(sample,lambda);
sample=input('Enter sample name - ', 's');
[Rm5,angle5]=reflmeas(sample,lambda);
sample=input('Enter sample name - ', 's');
[Rm6,angle6]=reflmeas(sample,lambda);

%constants from fitting thinnest sample with just UO2 layer.
stuffdb=[46 .0071 .0022; 56 .0114 .0038; 68 .0177 .0074; 85 ...
        .0306 .0238;100 .0364 .06; 115 -.025 .0243; 140 ...
        .0195 .0397; 155 .0308 .0272;175 .0381 .0296];
```

```
%find the right wavelength
index=1;
while stuffdb(index,1)<lambda
    index=index+1;
end

stuffd=stuffdb(index,2);
stuffb=stuffdb(index,3);

[uo2di,uo2bi]=uo2const(lambda); %if fitting this

%If you want to enter thicknesses for SiO2 and the oxide
%layer, use the first row.  If you want the numbers used
%in the thesis analysis, use the next three rows.
%thick=input('Enter thicknesses of SiO2 and stuff layers
             %in angstroms as [SiO2 stuff] - ');
sio2t=15.5;
oxidet=50;
thick=[sio2t oxidet];

%constant-total thickness of UO2+stuff
filmthick=[50 110 185 225 250 35];
stufft=oxidet;
uo2thick=filmthick;
%put here the things you want to fit
fitconsti=[uo2di uo2bi stuffd stuffb];

Rcinit1=calcrefl(fitconsti,lambda,angle1,thick,uo2thick(1));
Rcinit2=calcrefl(fitconsti,lambda,angle2,thick,uo2thick(2));
Rcinit3=calcrefl(fitconsti,lambda,angle3,thick,uo2thick(3));
Rcinit4=calcrefl(fitconsti,lambda,angle4,thick,uo2thick(4));
Rcinit5=calcrefl(fitconsti,lambda,angle5,thick,uo2thick(5));
Rcinit6=calcrefl(fitconsti,lambda,angle6,thick,uo2thick(6));

fprintf('Press Enter to Continue');
pause
option=optimset('TolX',1e-5);
tic
uo2db=fminsearch('leastsq',fitconsti,option,Rm1,Rm2,Rm3,...
    Rm4,Rm5,Rm6,lambda,angle1,angle2,angle3,angle4,angle5,...
    angle6,thick,uo2thick);
toc
```

```
UO2delta=uo2db(1)
UO2beta=uo2db(2)
stuffdelta=uo2db(3)
stuffbeta=uo2db(4)
%If you are fitting the thickness of the oxide layer
%use the next row.
%stuffthick=uo2db(5)

Rc1=calcrefl(uo2db,lambda,angle1,thick,uo2thick(1));
Rc2=calcrefl(uo2db,lambda,angle2,thick,uo2thick(2));
Rc3=calcrefl(uo2db,lambda,angle3,thick,uo2thick(3));
Rc4=calcrefl(uo2db,lambda,angle4,thick,uo2thick(4));
Rc5=calcrefl(uo2db,lambda,angle5,thick,uo2thick(5));
Rc6=calcrefl(uo2db,lambda,angle6,thick,uo2thick(6));
figure(5)
plot(angle2,Rm2,angle2,Rc2)
axis([0 max(angle2) 0 1])
xlabel('Grazing Angle')
ylabel('Reflection')
title(['Sample UO12, \lambda = ',int2str(lambda),' ...
    Angstroms, Final Fit'])
figure(6)
plot(angle3,Rm3,angle3,Rc3)
axis([0 max(angle3) 0 1])
xlabel('Grazing Angle')
ylabel('Reflection')
title(['Sample UO13, \lambda = ',int2str(lambda),' ...
    Angstroms, Final Fit'])
figure(7)
plot(angle4,Rm4,angle4,Rc4)
axis([0 max(angle4) 0 1])
xlabel('Grazing Angle')
ylabel('Reflection')
title(['Sample UO14, \lambda = ',int2str(lambda),' ...
    Angstroms, Final Fit'])
figure(8)
plot(angle5,Rm5,angle5,Rc5)
axis([0 max(angle5) 0 1])
xlabel('Grazing Angle')
ylabel('Reflection')
title(['Sample UO15, \lambda = ',int2str(lambda),' ...
    Angstroms, Final Fit'])
figure(9)
```

```
plot(angle1,Rm1,angle1,Rc1)
axis([0 max(angle1) 0 1])
xlabel('Grazing Angle')
ylabel('Reflection')
title(['Sample UO11, \lambda = ',int2str(lambda),' ...
    Angstroms, Final Fit'])
figure(10)
plot(angle6,Rm6,angle6,Rc6)
axis([0 max(angle6) 0 1])
xlabel('Grazing Angle')
ylabel('Reflection')
title(['Sample UO16, \lambda = ',int2str(lambda),' ...
    Angstroms, Final Fit'])
```

File reflmeas.m is set up to calculate the reflection of the measured data taken at ALS. The file names are included in the program and it is set up to calculate the reflection for all six samples. The code for reflmeas.m is as follows:

```
%So far this program will calculate and display the reflection
%of one sample if the file names and sample name are read in.
function [refl,angle]=reflmeas(name,lambda)

%read in all of the data files from ALS.
if lambda==46
    if name=='UO11'
        anglescan='uox000176.dat';
        I0='uox000178.dat';
    elseif name=='UO12'
        anglescan='uox000289.dat';
        I0='uox000286.dat';
    elseif name=='UO13'
        anglescan='uox000299.dat';
        I0='uox000293.dat';
    elseif name=='UO14'
        anglescan='uox000195.dat';
        I0='uox000192.dat';
    elseif name=='UO15'
        anglescan='uox000200.dat';
        I0='uox000197.dat';
    elseif name=='UO16'
        anglescan='uox000249.dat';
        I0='uox000244.dat';
    end
elseif lambda==56
```

```
    if name=='UO11'
        anglescan='uox000175.dat';
        I0='uox000178.dat';
    elseif name=='UO12'
        anglescan='uox000288.dat';
        I0='uox000286.dat';
    elseif name=='UO13'
        anglescan='uox000298.dat';
        I0='uox000293.dat';
    elseif name=='UO14'
        anglescan='uox000194.dat';
        I0='uox000192.dat';
    elseif name=='UO15'
        anglescan='uox000199.dat';
        I0='uox000197.dat';
    elseif name=='UO16'
        anglescan='uox000248.dat';
        I0='uox000244.dat';
    end
elseif lambda==68
    if name=='UO11'
        anglescan='uox000177.dat';
        I0='uox000178.dat';
    elseif name=='UO12'
        anglescan='uox000287.dat';
        I0='uox000286.dat';
    elseif name=='UO13'
        anglescan='uox000297.dat';
        I0='uox000293.dat';
    elseif name=='UO14'
        anglescan='uox000193.dat';
        I0='uox000192.dat';
    elseif name=='UO15'
        anglescan='uox000198.dat';
        I0='uox000197.dat';
    elseif name=='UO16'
        anglescan='uox000247.dat';
        I0='uox000244.dat';
    end
elseif lambda==85
    if name=='UO11'
        anglescan='uox000164.dat';
        I0='uox000165.dat';
```

```
    elseif name=='UO12'
        anglescan='uox000145.dat';
        I0='uox000146.dat';
    elseif name=='UO13'
        anglescan='uox000058.dat';
        I0='uox000065.dat';
    elseif name=='UO14'
        anglescan='uox000190.dat';
        I0='uox000191.dat';
    elseif name=='UO15'
        anglescan='uox000212.dat';
        I0='uox000209.dat';
    elseif name=='UO16'
        anglescan='uox000242.dat';
        I0='uox000243.dat';
    end
elseif lambda==100
    if name=='UO11'
        anglescan='uox000163.dat';
        I0='uox000161.dat';
    elseif name=='UO12'
        anglescan='uox000144.dat';
        I0='uox000146.dat';
    elseif name=='UO13'
        anglescan='uox000062.dat';
        I0='uox000065.dat';
    elseif name=='UO14'
        anglescan='uox000189.dat';
        I0='uox000191.dat';
    elseif name=='UO15'
        anglescan='uox000211.dat';
        I0='uox000209.dat';
    elseif name=='UO16'
        anglescan='uox000241.dat';
        I0='uox000243.dat';
    end
elseif lambda==125
    if name=='UO11'
        anglescan='uox000159.dat';
        I0='uox000160.dat';
    elseif name=='UO12'
        anglescan='uox000139.dat';
        I0='uox000140.dat';
```

```
    elseif name=='U013'
        anglescan='uox000049.dat';
        I0='uox000050.dat';
    elseif name=='U014'
        anglescan='uox000185.dat';
        I0='uox000186.dat';
    elseif name=='U015'
        anglescan='uox000224.dat';
        I0='uox000225.dat';
    elseif name=='U016'
        anglescan='uox000231.dat';
        I0='uox000234.dat';
    end
elseif lambda==140
    if name=='U011'
        anglescan='uox000158.dat';
        I0='uox000160.dat';
    elseif name=='U012'
        anglescan='uox000138.dat';
        I0='uox000140.dat';
    elseif name=='U013'
        anglescan='uox000032.dat';
        I0='uox000035.dat';
    elseif name=='U014'
        anglescan='uox000184.dat';
        I0='uox000186.dat';
    elseif name=='U015'
        anglescan='uox000223.dat';
        I0='uox000225.dat';
    elseif name=='U016'
        anglescan='uox000230.dat';
        I0='uox000227.dat';
    end
elseif lambda==155
    if name=='U011'
        anglescan='uox000157.dat';
        I0='uox000160.dat';
    elseif name=='U012'
        anglescan='uox000137.dat';
        I0='uox000134.dat';
    elseif name=='U013'
        anglescan='uox000033.dat';
        I0='uox000035.dat';
```

```
    elseif name=='U014'
        anglescan='uox000183.dat';
        I0='uox000186.dat';
    elseif name=='U015'
        anglescan='uox000222.dat';
        I0='uox000225.dat';
    elseif name=='U016'
        anglescan='uox000229.dat';
        I0='uox000227.dat';
    end
elseif lambda==175
    if name=='U011'
        anglescan='uox000156.dat';
        I0='uox000153.dat';
    elseif name=='U012'
        anglescan='uox000136.dat';
        I0='uox000134.dat';
    elseif name=='U013'
        anglescan='uox000034.dat';
        I0='uox000035.dat';
    elseif name=='U014'
        anglescan='uox000182.dat';
        I0='uox000181.dat';
    elseif name=='U015'
        anglescan='uox000221.dat';
        I0='uox000217.dat';
    elseif name=='U016'
        anglescan='uox000228.dat';
        I0='uox000227.dat';
    end
end

[ang diode m3 current] = textread(anglescan,'%f %f %f %f',...
    'headerlines',1); %read in angle scan
%interpolate angle scan
num=1;
while ang(num)<2
    num=num+1;
end
M=length(ang);

angle=ang(num:M);
```

```
[wave zdi zm zcur] = textread(I0,'%f %f %f %f',...
    'headerlines',1);
p=1;
while wave(p)<lambda
    p=p+1;
end
zdiode=zdi(p);
zm3=zm(p);
zcurrent=zcur(p);

%now calculate the reflection
refl=diode(num:M)./zdiode.*zm3./m3(num:M);
plot(angle,refl,'-b','LineWidth',1.5)
axis([0 90 0 1])
```

The file calcrefl.m calculates the reflection of samples using the Parratt recursion formulas and Fresnel coefficients. The code for calcrefl.m is:

```
%This file will calculate the refl. of a multilayer.
%Source is from the appendix in Shannon's honors thesis

function R=calcrefl(fitconst,lambda,angle,thick,uo2t)
%This uses the Parratt recursion formula.
%fitconst are the constants we are fitting, stuff delta beta
%and uo2 delta beta
%thick is SiO2 and initial stuff
%uo2t is the uo2+stuff total thickness

D=zeros(1,5);
D(2)=thick(1); %sio2 layer
%constrain the oxide layer to only be total thickness
if uo2t>thick(2)
    D(3)=uo2t-thick(2); %uo2 layer
    D(4)=thick(2); %stuff layer
else
    D(3)=0; %uo2 layer
    D(4)=uo2t; %stuff layer
end

%grazing angle in degrees converted to radians
theta=angle*pi/180;
N=length(D); %number of layers in mirror, including vacuum
Nt=length(theta);
rs=zeros(Nt,N); %initialize
```

```
rp=zeros(Nt,N); %initialize
k=2*pi/lambda; %calculate wavenumber

%read the optical constants as delta and beta from files
[sid,sib]=siconst(lambda);
[sio2d,sio2b]=sio2const(lambda);

uo2d=fitconst(1); %if fitting these
uo2b=fitconst(2); %if fitting these
stuffd=fitconst(3); %if fitting these
stuffb=fitconst(4); %if fitting these

delta=[sid sio2d uo2d stuffd 0]; %[Si SiO2 layer stuff vacuum]
beta=[sib sio2b uo2b stuffb 0];  %[Si SiO2 layer stuff vacuum]
n=1-delta+i*beta;

for t=1:Nt
%These are factors needed for Fresnel and Parratt.
sinth(t,1:N)=sqrt(n(1,1:N).^2-(cos(theta(t,1)))^2);
kz(t,1:N)=k*sinth(t,1:N);
C4(t,1:N)=exp(i*kz(t,1:N).*D(1,1:N)*2);

%Fresnel for s polarization
fs(t,1:N-1)=(sinth(t,2:N)-sinth(t,1:N-1))./(sinth(t,2:N)+...
    sinth(t,1:N-1));
%Fresnel for p polarization
fp(t,1:N-1)=(n(1,1:N-1).^2.*sinth(t,2:N)-n(1,2:N).^2.*...
    sinth(t,1:N-1))./(n(1,1:N-1).^2.*sinth(t,2:N)+n(1,2:N)...
    .^2.*sinth(t,1:N-1));

for w=1:N-1
rs(t,w+1)=C4(t,w+1).*(fs(t,w)+rs(t,w))./(1+fs(t,w).*rs(t,w));
rp(t,w+1)=C4(t,w+1).*(fp(t,w)+rp(t,w))./(1+fp(t,w).*rp(t,w));
%Parratt recursions
end
end

%These are really Rsprime and Rpprime but for last layer C=1
%so Rprime=R*C^2 becomes Rprime=R
Rs=(abs(rs(1:Nt,N))).^2; %reflection from s polarization
Rp=(abs(rp(1:Nt,N))).^2; %reflection from p polarization
R=(.1*Rp+.9*Rs);%total reflection for unpolarized light
```

File leastsq.m is called from fitrefl.m using fminsearch:

```
function s=leastsq(fitstuff,Rm1,Rm2,Rm3,Rm4,Rm5,Rm6,lambda,...
    angle1,angle2,angle3,angle4,angle5,angle6,thick,uo2t)

%leastsq can be passed to fminserach to do a
%non-lineasr least squares fit of the funciton
%funcfit(a,x) to the data set (x,y).
%funcfit.m is built by the user

%a is a vector of variable parameters; x and y
%are the arrays of data points2

s1=sum((Rm1-calcrefl(fitstuff,lambda,angle1,thick,uo2t(1))).^2);
s2=sum((Rm2-calcrefl(fitstuff,lambda,angle2,thick,uo2t(2))).^2);
s3=sum((Rm3-calcrefl(fitstuff,lambda,angle3,thick,uo2t(3))).^2);
s4=sum((Rm4-calcrefl(fitstuff,lambda,angle4,thick,uo2t(4))).^2);
s5=sum((Rm5-calcrefl(fitstuff,lambda,angle5,thick,uo2t(5))).^2);
s6=sum((Rm6-calcrefl(fitstuff,lambda,angle6,thick,uo2t(6))).^2);
s=s1+s2+s3+s4+s5+s6

return

%need to use this with fminsearch
```

The following files find the calculated optical constants from atomic scattering factors obtained from CXRO [17]. The files are the same for each material with the name in textread changed. The files are: siconst.txt, sio2const.txt, and uo2const.txt.

```
function [delta,beta]=siconst(lambda)
%This function will work with calcrefl.m to calculate the
%reflection of a multilayer.

%data is from cxro web page
[w d b] = textread('siconst.txt','%f %f %f','headerlines',2);
xi=1:.1:length(w);
wave=interp1(w,xi','linear')*10;
delt=interp1(d,xi','linear');
bet=interp1(b,xi','linear');

m=1;
while wave(m)<lambda
    m=m+1;
```

```
end

delta=delt(m);
beta=bet(m);
```

The code to calculate the χ^2 error used the same code as above with the following difference in the fit code:

```
function f=errorfit(fitstuff,Rm1,Rm2,Rm3,Rm4,Rm5,Rm6,lambda,...
    angle1,angle2,angle3,angle4,angle5,angle6,thick,uo2t,...
    chi0sq,sigmasq);

s1=sum((Rm1-calcrefler(fitstuff,lambda,angle1,thick,...
    uo2t(1))).^2);
s2=sum((Rm2-calcrefler(fitstuff,lambda,angle2,thick,...
    uo2t(2))).^2);
s3=sum((Rm3-calcrefler(fitstuff,lambda,angle3,thick,...
    uo2t(3))).^2);
s4=sum((Rm4-calcrefler(fitstuff,lambda,angle4,thick,...
    uo2t(4))).^2);
s5=sum((Rm5-calcrefler(fitstuff,lambda,angle5,thick,...
    uo2t(5))).^2);
s6=sum((Rm6-calcrefler(fitstuff,lambda,angle6,thick,...
    uo2t(6))).^2);
s=s1+s2+s3+s4+s5+s6;
chisq=s/sigmasq;
f=(chisq-chi0sq-1)^2;

return
```

The values used for the optical constants of Si, SiO_2 and UO_2 are all taken from the CXRO web page [17].

Bibliography

[1] D. Attwood, *Soft X-rays and Extreme Ultraviolet Radiation* (Cambridge University Press, Cambridge, 1999), pp. 59-61, 371.

[2] D. Attwood, *Soft X-ray Microscopy and EUV Lithography: Imaging in the 20-50nm Region* colloquium given Jan 9, 2002 at Brigham Young University Dept. of Physics and Astronomy.

[3] Y. Horikawa, K. Nagai, Y. Iketaki, "Soft x-ray reflectometry with a laser-produced plasma source." *Optical Engineering*, **33** (5), 1721-5 (1994).

[4] B. R. Sandel *et. al.* "The Extreme Ultraviolet Imager Investigation for the IMAGE Mission." *Space Science Reviews* **91** (1-2), 197-242 (2000).

[5] W. Cash (private comunication, 2002).

[6] M. B. Squires, Honors Thesis, Brigham Young University, 1999.

[7] D. T. Oliphant, M. S. Thesis, Brigham Young University, 2000.

[8] J. H. Weaver, C. Krafka, D. W. Lynch, E. E. Koch, *Optical Properties of Metals in Physics Data*, (Fachinformationszentrum, Karlsruhe, 1981), Vols. I, II.

[9] B. L. Henke, E. M. Gullikson, and J. C. Davis, "X-ray interactions: photoabsorption, scattering, transmission, and reflection at E=50-30000 eV, Z=1-92", *Atomic Data and Nuclear Data Tables*, **54** (2), 181-342 (1993).

[10] C. T. Chantler, "Theoretical Form Factor, Attenuation, and Scattering Tabulation for Z=1-92 from E=1-10 eV to E=0.4-1.0 MeV." *J. Phys. Chem., Ref. Data*, **24** (1), 71-643 (1995).

[11] J. Naegele, L.Manes, U. Birkholz, "Optical properties of UO_2 and U_4O_9 single crystals and their relation to chemical bonding." *Plutonium and Other Actinides*, edited by H. Blank and R. Lindner (North-Holland, Amsterdam, 1976), pp. 393-408.

[12] T. R. Griffiths and H. V. St. Aubyn Hubbard, "Absorption spectrum of single-crystal UO_2: Identification of and effect of temperature on the peak positions of essentially all optical transitions in the visible to near infrared regions using derivative spectroscopy." *Journal of Nuclear Materials*, **185**, 243-59 (1991).

[13] J. Schoenes, "Optical Properties and Electronic Structure of UO_2." *J. Appl. Phys.*, **49**, 1463-5 (1978).

[14] H. V. St. Aubyn Hubbard and T. R. Griffiths, "An Investigation of Defect Structures in Single-crystal UO_{2+x} by Optical Absorption Spectroscopy." *J. Chem. Soc., Faraday Trans. 2*, **83**, 1215-27 (1987).

[15] R. J. Ackermann, R. J. Thorn, G. H. Winslow, "Visible and UV Absorption Properties of UO_2 Films." *J. Optical Soc. Am.*, **49** (11), 1107-12 (1959).

[16] A. Companion and G. H. Winslow, "Diffuse Reflectance Measurements on Bulk Urnaium Dioxide." *J. Opt. Soc. Am.*, **50**, 1043-5 (1960).

[17] http://www-cxro.lbl.gov/optical_constants/getdb2.html, May 23, 2002.

[18] E. Spiller, *Soft X-ray Optics* (SPIE Optical Engineering Press, Bellingham, 1994), pp. 106.

[19] S. Lunt, R. S. Turley, D. D. Allred, "Design of bifunctional XUV multilayer mirrors using a genetic algorithm." *Journal of X-Ray Science and Technology*, **9**, 1-11 (2001).

[20] J. D. Jackson, *Classical Electrodynamics*, 3rd ed. (John Wiley & Sons, Inc., New York, 1999), pp. 333-5.

[21] G. B. Arfken and H. J. Weber, *Mathematical Methods for Physicists*, 5th ed. Harcourt/Academic Press, San Diego, 2001, p. 473.

[22] M. Ohring, *The Material Science of Thin Films* (Academic Press, San Diego, 1992).

[23] D. L. Windt, "IMD - software for modeling the optical properties of multilayer films." *Computers in Physics*, **12** (4), 360-70 (1998).

[24] J. A. Woollam, Co., Inc., *Guide to Using WVASE32^{TM}*, p. 20.

[25] http://www.jawoollam.com/m2000.html, June 14, 2002.

[26] J. H. Weaver, "Low-energy optical absorption in α-U metal." *J. Opt. Soc. Am.*, **70** (8), 1030-1 (1980).

[27] G. C. Allen and N. R. Holmes, "Surface Characterisation of α-, β-, γ-, and δ-UO_3 using X-ray Photoelectron Spectroscopy." *J. Chem. Soc. Dalton Trans.*, **12**, 3009-15 (1987).

[28] A. S. Baev, Yu. A. Teterin, L. G. Mashirov, and D. N. Suglobov, "X-ray Photoelectron Investigation of Uranium Compounds." *Soviet Radiochemistry*, **28** (4), 418-425 (1986).

[29] Yu. A. Teterin, "Structure of X-ray photoelectron, emission, and conversion spectra and molecular orbitals of uranium compounds." *Journal of Structural Chemistry*, **39** (6), 850-6 (1998).

[30] B. W. Veal and D. J. Lam, "X-ray photoelectron studies of thorium, uranium, and their dioxides." *Physical Review B*, **10** (12), 4902-8 (1974).

[31] L. E. Cox, "XPS Evidence for 5f Bonding Participation in UO_2." *Journal of Electron Spectroscopy and Related Phenomena*, **26**, 167-71 (1982).

[32] K. Winer, C. A. Colmenares, R. L. Smith, and F. Wooten, "On the Stability of Sub-stoichiometric Uranium Oxides." *Surface Science*, **177**, 484-92 (1986).

[33] J. J. Pireaux *et. al.* "Shake-up Satellites in the X-ray photoelectron spectra of uranium oxides and fluorides. A Band Structure Scheme for uranium dioxide, UO_2." *Chemical Physics*, **22**, 113-20 (1977).

[34] Yu. A. Teterin *et. al.* "The Role of the U6p,5f electrons in chemical bonding of uranyl and uranium fluorides: X-ray photoelectron and X-ray emission studies." *Journal of Electron Spectroscopy and Related Phenomena*, **114-6**, 915-23 (2001).

[35] Yu. A. Teterin *et. al.* "A Study of Synthetic and Natural Uranium Oxides by X-ray Photoelectron Spectroscopy." *Phys. Chem. Minerals* **7**, 151-8 (1981).

[36] R. J. Thorn, "Intensities and Satellites of 4f-photoelectrons in Thorium and Uranium Dioxides." *J. Phys. Chem. Solids*, **43** (6), 571-5 (1982).

[37] Yu. A. Teterin *et. al.* "Inner valence molecular orbitals and structure of the X-ray $O_{4,5}$(Th,U) emission spectra in thorium and uranium oxides." *Journal of Electron Spectroscopy and Related Phenomena*, **96**, 229-36 (1998).

[38] http://goliath.inrs-ener.uquebec.ca/surfsci/arxps/sampling.html, July 31, 2002.

[39] D. G. Stearns, "X-ray scattering from interfacial roughness in multilayer structures." *J. Appl. Phys.*, **71** (9), 4286-98 (1992).

[40] M. B. Squires, M. S. Thesis, Brigham Young University, 2001.

[41] M. B. Squires, D. D. Allred, and R. S. Turley, "The Optical Constants of Sputtered U and a-Si at 30.4 and 58.4 nm." *Proc. of SPIE - Inte. Society for Optical Eng.*, **3767**, 288-94 (1999).

[42] Å. Fäldt and P. O. Nilsson, "Optical Properties of uranium in the range 0.6-25 eV." *Journal of Physics F: Metal Physics*, **10** (11), 2573-80 (1980).

[43] http://www-cxro.lbl.gov/als6.3.2/, June 24, 2002.

[44] J. H. Underwood *et. al.* “Calibration and standards beamline 6.3.2 at the Advanced Light Source.” *Rev. Sci. Instrum.*, **67** (9), 1-5 (1996).

[45] V. G. Kohn, “On the theory of reflectivity by an x-ray multilayer mirro.” *Phys. Stat. Sol. (b)* **187** (61), 61-70 (1995).

[46] L. G. Parratt, “Surface Studies of Solids by Total Reflection of X-rays.” *Physical Review* **95** (2), 359-69 (1954).